Comparing Eurocode 8-5 and AASHTO methods for earth pressure analysis against centrifuge tests, finite elements, and the Generalized Coefficients of Earth Pressure

Lysandros Pantelidis (lysandros.pantelidis@cut.ac.cy)
Cyprus University of Technology https://orcid.org/0000-0001-5979-6937
Panagiotis Christodoulou
Cyprus University of Technology https://orcid.org/0000-0002-3238-2504

Research Article

Keywords: Active Earth Pressure, Passive Earth Pressure, Eurocode 8-5, EN 1998-5, Numerical Validation, The Generalized Coefficients of Earth Pressure

Posted Date: October 25th, 2022

DOI: https://doi.org/10.21203/rs.3.rs-1808466/v3

Comparing Eurocode 8-5 and AASHTO methods for earth pressure analysis against centrifuge tests, finite elements, and the Generalized Coefficients of Earth Pressure

Lysandros Pantelidis[1,*], Panagiotis Christodoulou[1]

[1] Cyprus University of Technology, 3036 Limassol, CY

* lysandros.pantelidis@cut.ac.cy

v2 (31/07/2022): The authors checked all table values; some very minor differences were observed and corrected. Also, the wording was improved in lines 190-194.

v3 (25/10/2022): The authors deleted the section with title „Replacing $\{c', \varphi', k_h\}$ with the mid-height $\{c_m, \varphi_m\}$ones and k_h=0 in slope stability problems" for giving a paper oriented exclusively to earth pressures and also, for reducing its size. The application of the proposed earth pressure theory to the slope stability problem is an interesting task and subject matter of future work. Two more citations have also been added (see citations [3] and [4] in the current version). Finally, the prEN1998-5:2021 was updated to prEN1998-5:2022.

Abstract

This paper presents an exhaustive comparison of the earth pressure methods included in EN1998-5:2004 (use of Mononobe-Okabe method, M-O), prEN1998-5:2022 and AASHTO (M-O with half peak ground acceleration) standards, against contemporary centrifuge tests, finite elements, and the method proposed by the first author in 2019. The latter is a continuum mechanics approach for deriving earth pressure coefficients for any soil state between the "at-rest" state and the active or passive state, applicable to cohesive-frictional soils and both horizontal and vertical pseudo-static conditions. The same method also provides analytical expressions for the calculation of the required wall movement for the mobilization of the active (or passive) failure state, as well as for the mobilized shear strength values of soil. The comparison includes among others, centrifuge test results from two different studies, and results from 157 finite element models from two different programs. All experimental, numerical, and analytical results show that the EN19985-5:2004 method gives conservative to excessively conservative active earth pressure values, AASHTO's approach fairly good behavior, while prEN1998-5:2022 excessively conservative values. For the passive state, all methods included in the

above-mentioned standards, return unreliable and unconservative results. In contrast, the results obtained by the proposed method show a remarkable agreement with the respective ones obtained both by the finite element method and the various centrifuge tests. Also, it is shown that a pseudo-static earth retention analysis, can be replaced by a respective static analysis, just substituting the (c', φ') values of soil of the original problem with the mobilized ones.

Keywords: Active Earth Pressure, Passive Earth Pressure, Eurocode 8-5, EN 1998-5, Numerical Validation, The Generalized Coefficients of Earth Pressure

1 Introduction

Three analytical methods for the calculation of earth pressures are compared in this paper. The first refers to a method proposed recently by the first author [1]. This is a continuum mechanics approach for deriving earth pressure coefficients for any soil state between the "at-rest" state and the active or passive state, applicable to cohesive-frictional soils and both horizontal and vertical pseudo-static conditions. It is worth mentioning that under static conditions this rather complicated analysis based on Cauchy's first law of motion (extended suitably to deformable bodies with internal resistance) leads to the well-known Rankine's expression for cohesive-frictional soils for the active state. By just changing the arithmetic value of a controlling parameter from infinity to 1, the same approach (again under static conditions) leads to Jaky's [2] well-known $Ko = 1 - \sin\varphi'$ expression for the earth pressure at-rest with an additional term for the cohesion of soil. The same method also provides analytical expressions for the calculation of the required wall movement Δx_{max} for the mobilization of the active or passive failure state in case of smooth or rough walls. Informatively, the proposed method has

already been applied to axially loaded piles in $c' - \varphi'$ soils [3] and embedded retaining walls [4] with great success. The basic expressions are summarized below.

The generalized coefficient of earth pressure at-rest is:

$$K_{OE} = (1 - \sin\varphi')(1 + \tan\theta_1 \cdot \tan\varphi') - \frac{1}{1-k_v}\frac{2c_m}{\gamma z}\tan\left(45^o - \frac{\varphi'}{2}\right) \quad (1)$$

The generalized coefficient of active or passive earth pressure (denoted by the letter A or P respectively) is:

$$K_{(A/P)E} = \frac{1 \mp \sin\varphi'}{1 \pm \sin\varphi'}(1 \pm 2 \cdot \tan\theta_1 \cdot \tan\varphi') \mp \frac{1}{1-k_v}\frac{2c_m}{\gamma z}\tan\left(45^o \mp \frac{\varphi'}{2}\right) \quad (2)$$

(the readers may find more interesting the general form for the above equations given in Pantelidis [4]).

The earth pressure at any of the above states (active / at-rest / passive) at depth z, therefore, is

$$\sigma_{(A/O/P)E} = K_{(A/O/P)E}(1 - k_v)\gamma z \quad (3)$$

while the maximum horizontal displacement (at depth z) for the mobilization of the active or passive state is

$$\Delta x_{max} = \frac{\pi}{4}\frac{(1-\nu^2)}{E_s}\frac{(1+z/H)^3(1-z/H)}{z/H}H \cdot \Delta K \cdot (1 - k_v)\gamma z \quad (4)$$

Pantelidis' [1] has provided formulae for the analytical calculation of the mobilized shear strength parameters of soil. Alternatively, can be calculated through relevant charts (also available in [1]). For purely frictional soils, the mobilized friction angle can be calculated by the following expressions:

$$\varphi_{m(O)} = ArcSin\left[\frac{1-(1-\sin\varphi\prime)(1+\tan\theta_1\tan\varphi\prime)}{1+(1-\sin\varphi\prime)(1+\tan\theta_1\tan\varphi\prime)(1-\sin\varphi\prime)}\right] = \mathrm{ArcSin}\left[\frac{1-K_{OE(\,c'=0)}}{1+K_{OE(\,c'=0)}\cdot K_{O(Jaky'_S)}}\right] \quad (5)$$

$$\varphi_{m(A/P)} = \pm\left\{90^o - 2\,\mathrm{Arctan}\left[\tan\left(45^o \mp \frac{\varphi'}{2}\right)\sqrt{1 \pm 2\frac{k_h}{1-k_v}\tan\varphi'}\right]\right\} \quad (6)$$

while the K_{AE} and K_{PE} coefficients simplify to:

$$K_{(A/P)E} = \frac{1\mp\sin\varphi_m}{1\pm\sin\varphi_m} = \frac{1\mp\sin\varphi\prime}{1\pm\sin\varphi\prime}\left(1 \pm 2\frac{k_h}{1-k_v}\tan\varphi'\right) \quad (7)$$

The second analytical method is the Mononobe-Okabe method [5–7] which has been adopted by the current Eurocode 8-5 standard (denoted as normative in EN1998-5:2004 [8]) as well as AASHTO [9]. According to Mononobe-Okabe, the coefficient of active (or passive) earth pressure is:

$$K_{(A/P)E} = \frac{\cos^2(\varphi'-\theta_1\mp\beta)}{\cos\theta_1\cdot\cos^2\beta\cdot\cos(\delta\pm\beta+\theta_1)\left[1\pm\sqrt{\frac{\sin(\varphi'+\delta)\cdot\sin(\varphi'-\theta_1\mp a_S)}{\cos(\delta\pm\beta+\theta_1)\cdot\cos(a_S-\beta)}}\right]^2} \quad (8)$$

The third analytical method is the one included in the draft standard prEN1998-5:2022 [10] (denoted as informative). The coefficient of active or passive earth pressure is:

$$K_{(A/P)E} = \left[\frac{\cos\delta\left(\cos\delta\mp\sqrt{\sin^2\varphi'-\sin^2\delta}\right)}{\cos(a_s\pm\theta_2)\pm\sqrt{\sin^2\varphi'-\sin^2(a_s\pm\theta_2)}}\right]\frac{\cos a_s}{\cos\theta_2}e^{\mp 2\psi_{(A/P)}\tan\varphi\prime} \quad (9)$$

with

$$\psi_{(A/P)} = 0.5\left\{\arcsin\left(\frac{\sin\delta}{\sin\varphi\prime}\right)\right\} \mp \arcsin\left[\frac{\sin(a_s\pm\theta_2)}{\sin\varphi\prime}\right] \mp \delta + a_s \mp \theta_2 \quad (10)$$

The active or passive earth pressure at depth z for the method included in EN1998-5:2004 standard is

$$\sigma_{(A/P)E} = K_{(A/P)E}(1 - k_v)\gamma z \quad (11)$$

while for the method included in prEN1998-5:2022 standard is

$$\sigma_{(A/P)E} = K_{(A/P)E}\gamma z \mp 2c'\sqrt{K_{(A/P)E}} \quad (12)$$

The EN1998-5:2004 standard does not have provision for soil's cohesion, while prEN1998-5:2022 ignores the vertical component of the seismic excitation.

For all methods, the resultant active or passive earth pressure force derives from the σ_{AE} (or σ_{PE} respectively) - z chart area:

$$P_{(A/P)E} = \int_H^0 \sigma_{(A/P)E} dz \quad (13)$$

Similarly, the resultant earth pressure at-rest force (proposed method) derives from the σ_{OE} - z chart area:

$$P_{OE} = \int_H^0 \sigma_{OE} dz \quad (14)$$

The square root of negative numbers in both EN1998-5:2004 and prEN1998-5:2022 standards (when $\varphi' - \theta_1 \mp a_s < 0$; the minus sign stands for the active state while the plus sign for the passive state), is arbitrarily and without any scientific basis replaced by unity. The Mononobe-Okabe method has also been adopted by AASHTO; AASHTO empirically reduces the Peak Ground Acceleration (PGA) to half its price (this is discussed later).

The validity of the above-mentioned analytical expressions is examined through several application examples, comparing analytical results with the respective numerical ones; besides finite elements are used to effectively simulate reality. Also, it is examined against contemporary centrifuge test results; centrifuge testing allows for creating a stress field in a model that

simulates prototype conditions in that proper scaling will provide correct strength and stiffness in granular soils [11]. Additional comparison examples are based on an in-situ measurement with press-in cell, and engineering experience; the latter refers to the Mononobe – Okabe method, as this has been empirically calibrated by AASHTO, as well as to U.S. Army Corps of Engineers' [12] Strength Mobilization Factor along Coulomb's failure surface for calculating the earth pressure at-rest using the active earth pressure coefficient.

In addition to examining the validity of the various earth pressure coefficients, the validation procedure is extended to the analytical expression for the calculation of the required wall movement for the mobilization of the active (or passive) failure state, as well as to the mobilized shear strength values of soil proposed by Pantelidis' [1].

2 Validation of the proposed earth pressure coefficients

2.1 Deriving Rankine's earth pressure expression through a continuum mechanic's approach

Rankine's and Coulomb's [13, 14] earth pressure theories are both well-established and widely adopted by engineers and academia. For frictionless (smooth), non-battered retaining walls with zero backfill inclination they return the same results, though Rankine's method calculates the active or passive earth pressure at point-level, while Coulomb's method gives directly the resultant active or passive earth pressure force. It is reminded that Rankine and Coulomb followed different paths for deriving their methods; in this respect, Rankine's method easily derives geometrically from Mohr circles combined with Mohr-Coulomb criterion, while Coulomb's method derives also geometrically, but from force polygon analysis.

On the other hand, the proposed method derives from a complicated continuum mechanics procedure, where an "internal resistance" term (in Mohr-Coulomb terms) has been added to Cauchy's first law of motion to extend its applicability to deformable bodies with internal resistance. The result is this expression:

$$K_{XE} = \frac{1-\sin\varphi'}{1+\sin\varphi'}\Big((1-\xi\cdot\sin\varphi') + \tan\theta_1\cdot\tan\varphi'\big(2+\xi\cdot(1-\sin\varphi')\big)\Big) - \frac{1}{1-k_v}\frac{2c_m}{\gamma z}tan\left(45^o-\frac{\varphi'}{2}\right) \quad (15)$$

with the soil state being undefined yet and $\xi = (1-3m)/\big(m\cdot(1+m)\big)$. The rather seemingly ambitious addition to a fundamental law of physics proved to be correct since, under static conditions and $m \to \infty$, Equation 15 leads to Rankine's expression for active earth pressures with Bell's extension for cohesion (see Figure 1). It is important to be mentioned that under static conditions, the calculated mobilized cohesion, c_m, is equal to its peak value, c' [1]. In addition to this, the proposed continuum mechanics approach allows for a deeper insight into the earth pressure theory indicating that the number "2" in Rankine-Bell's $2c'\sqrt{K_A}$ term [13, 15], represents the two horizontal planes of an infinitesimal cubic volume element resisting to shear in plane strain conditions. Furthermore, for cohesionless soils under static conditions, the very same equation (Equation 15) leads to Jaky's $K_O = 1-\sin\varphi'$ expression by setting $m \to 1$. It is therefore more than apparent that Equation 15 gives the earth pressure coefficient for any intermediate state simply changing the m value ($1 \le m \le \infty$). The full theory is described in detail in Pantelidis [1].

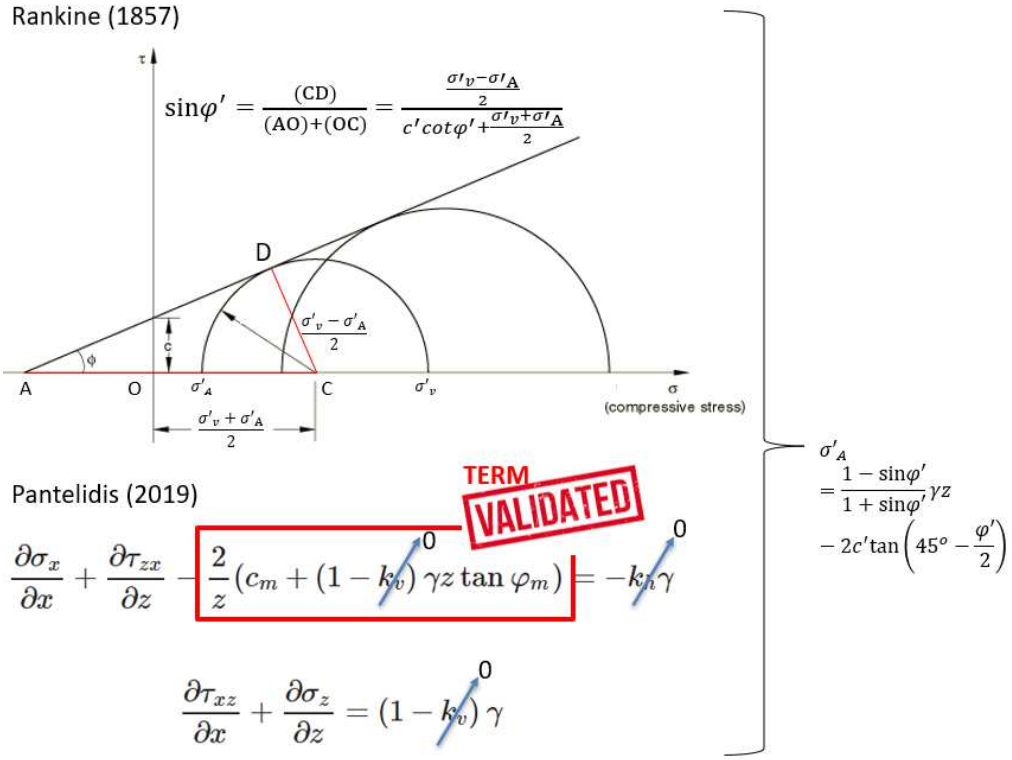

Figure 1. Validating Pantelidis' [1] internal resistance term in Cauchy's first law of motion.

2.2 Comparison against the empirical calibration of Mononobe – Okabe method by AASHTO

The last decades, a great number of experimental, numerical, and analytical studies [16–29] point that the Mononobe-Okabe method yields conservative active earth pressure values and excessively conservative values for *PGA* values greater than 0.4g. Some authorities have already recognized the conservatism of the Mononobe-Okabe method adopting as standard design practice the use of a reduction coefficient for the expected *PGA*; in this respect, AASHTO [9] considers a horizontal seismic coefficient equal to half *PGA*.

On the other hand, in addition to the fact that both methods included in EN1998-5:2004 and prEN1998-5:2022 standards present "negative root" when $\varphi' - \theta_1 \mp a_s < 0$ (minus for the

active and plus for the passive state), the active earth pressure coefficient of the prEN1998-5:2022 method appears to be even more conservative, as compared to the already conservative Mononobe-Okabe method. This is clearly shown in Figures 2a-2e for various k_h values ranging from 0.1 to 0.5 with 0.1 interval; these charts refer to non-battered, frictionless wall with zero backfill inclination. Two curves have been extended in Figure 2d to the undefined domain of friction angles ("negative root" problem) for illustration purposes. In this respect, each $K_{AE} - \varphi'$ curve has peak at $\varphi' = \theta_1$; for $0 \leq \varphi' < \theta_1$ the paradox of obtaining smaller K_{AE} coefficients for smaller φ' values is observed.

On the contrary, the empirical reduction of k_h by AASHTO [9] to its half value "sends" the corrected Mononobe - Okabe curves over author's fully analytical curves. This can be regarded strong evidence for the validity of the proposed method, springing from AASHTO experience. In addition, a no-shear-strength material (i.e., a material with zero cohesion and friction angle) exerts purely hydrostatic pressure on the wall and thus, all $K_{AE}- \varphi'$ curves must pass through the K=1 value (see the proposed curves in Figures 2a-2e or the aggregate chart of Figure 2f); the same stands for the passive state as well. Therefore, AASHTO curves rather need some "bending" so that to pass through the $\{K_{AE}$=1, φ'=0$\}$ point on the relevant charts.

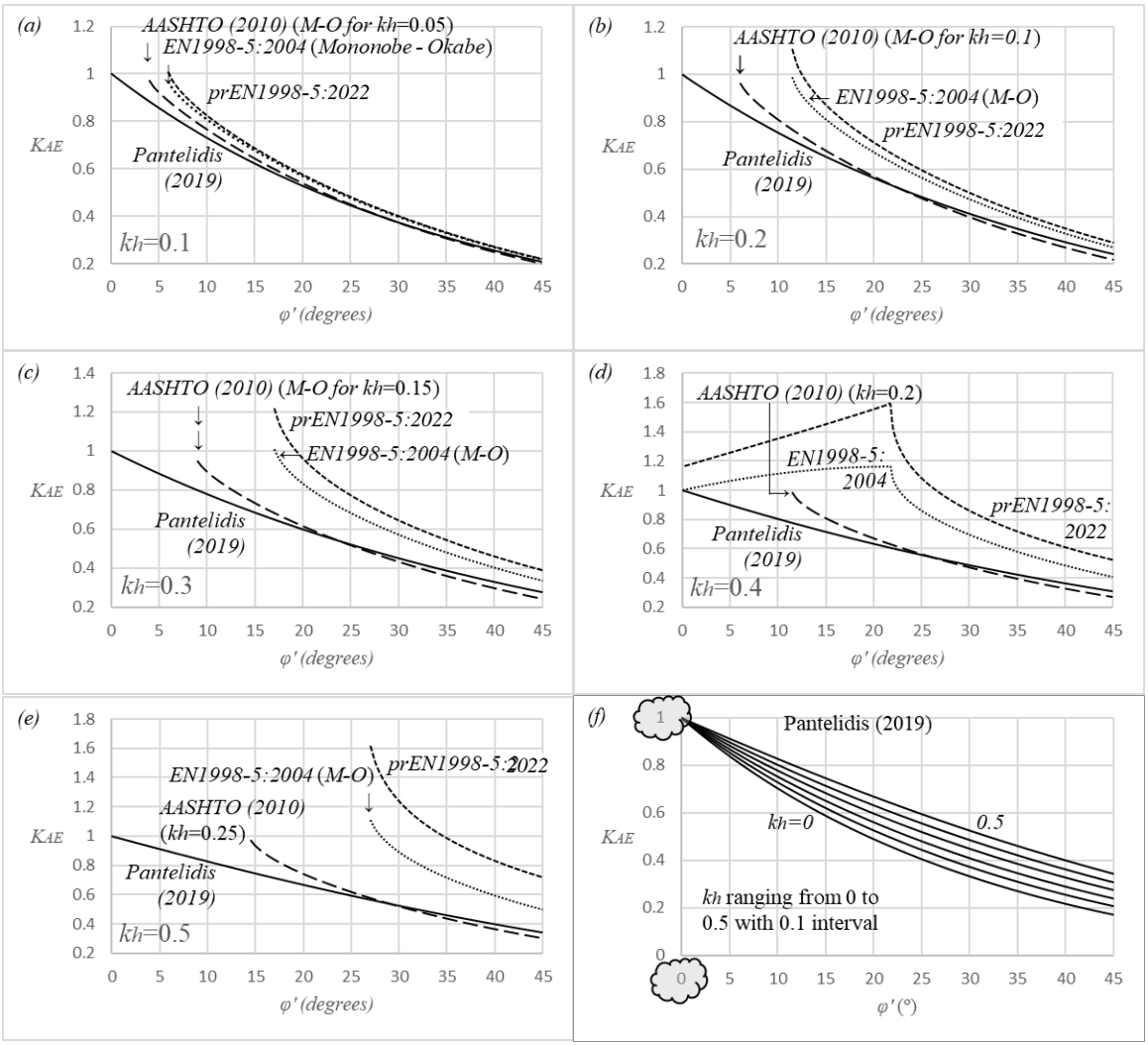

Figure 2. (a)-(e) Charts comparing the proposed method with the methods included in EN1998-5:2004 (M-O method), prEN1998-5:2022 and AASHTO (M-O method but for $PGA/2$) for k_h ranging from 0.1 to 0.5 with 0.1 interval. (f) Aggregate chart showing the curves derived by the proposed method. Charts referring to non-battered, frictionless wall with zero backfill inclination.

2.3 Comparison against numerical results

2.3.1 General

This section includes several numerical examples. The numerical results were obtained initially using the mrearth2d open-source, non-commercial finite element program developed by Prof. G. Fenton from Dalhousie University and Prof. D.V. Griffiths from Colorado School of Mines. The mrearth2d program was selected because its specialization to retaining walls offers convenience in modelling.

mrearth2d (freely available at http://www.engmath.dal.ca/rfem) is intended solely for the analysis of simple retaining walls (smooth or rough, non-battered walls with zero backfill inclination). A detailed description of the program can be found in [30–33]. Focusing on our deterministic analysis subject, the readers should skip the material referring to random fields, while it is noted that the horizontal pseudo-static function has been added by the authors (the vertical pseudo-static action just affects the unit weight of soil). The program was derived from the software published in the textbook by Smith and Griffiths [34]. All retaining walls studied herein correspond to a height of n elements; all elements are 8-noded, square with an edge of 0.1 m (e.g. a 3m-high wall consists of n=30 elements). For the active state the soil mass was discretized into 64 (horizontal) × 36 (vertical) elements. For the passive state the soil mass was discretized into 120×60 elements for three reasons: a) the passive failure mechanism affects greater soil mass, b) the compressive movement of the wall generates stresses in the soil which may return back, after bouncing on model's boundaries and c) the compressive action of the horizontal pseudo-static action against the boundary opposite the wall may also cause "action

and reaction" problem as mentioned in (b). For ensuring that the passive state cases were efficiently modelled, in addition to mrearth2d program, RocScience's RS2 program was used; RS2 is a commercial program for 2D finite element analysis of geotechnical structures for civil and mining applications.

Two mrearth2d models showing soil in its active and passive state are shown in Figure 3. mrearth2d uses a linear elastic, perfectly plastic Mohr–Coulomb constitutive model. The boundary conditions on the right side of the mesh (across the wall) are such that they allow vertical but not horizontal movement, while the base of the mesh is fully restrained. The top and left sides of the mesh are unrestrained, except for the nodes adjacent to the 'wall'. The active state against sliding is modeled by translating the nodes of the mesh next to the wall horizontally and uniformly away from the soil. These nodes have fixed horizontal components of displacement. As active or passive conditions are mobilized, the vertical components of these nodes are free to move vertically (perfectly smooth wall). The translational movement of the wall is performed incrementally. The finite element analysis is terminated when the active (or passive) state is reached (minimum or maximum action on the wall respectively). Regarding RS2, the mesh and boundary conditions are shown in Figure 4a; ten displacement increments were considered. Before solving with RS2, the models were checked statically for non-cohesionless soils under at-rest conditions if they return Jaky's $K_o \cdot \gamma \cdot z$ horizontal earth pressure throughout the soil mass (Figure 4b). The "comprehensive" type for convergence was used; according to RocScience, "checking force, energy and displacement criteria helps avoid false convergence. Furthermore, the maximum number of iterations was 1000, 6-noded triangular element with density 25 elements per square meter were used, the initial element loading was

231 "field stress and body force", while Jaky's $Ko = 1 - \sin\varphi'$ value was used as "stress ratio" in
232 the "field stress" menu. Of course, the problem studied herein is a plane-strain problem.

233 For all examples, the soil has unit weight 20 kN/m^3, modulus of elasticity 20,000 kPa and
234 Poisson's ratio 0.3, while the vertical seismic coefficient was set to zero (because k_v simply
235 affects the unit weight of soil in a $\gamma(1 - k_v)$ pseudo-static manner). The analysis refers to rigid,
236 non-battered, frictionless walls with zero backfill inclination as shown in Figures 3 and 4. Fully
237 drained conditions were considered.

238 A number of comparison tables are given throughout the present paper. The column num-
239 bering follows a cX.Y, notation with X and Y being the number of table and column respec-
240 tively. If a column is repeated in a subsequent table, the original numbering is used in it. The
241 numerical subscript under the *RD* symbol (relative difference) prompts to the P_{AE} or P_{PE} values
242 used as reference point (e.g. the $P_{AE,1}$ values were used as reference point for calculating the
243 RD_1 values and so on).

244

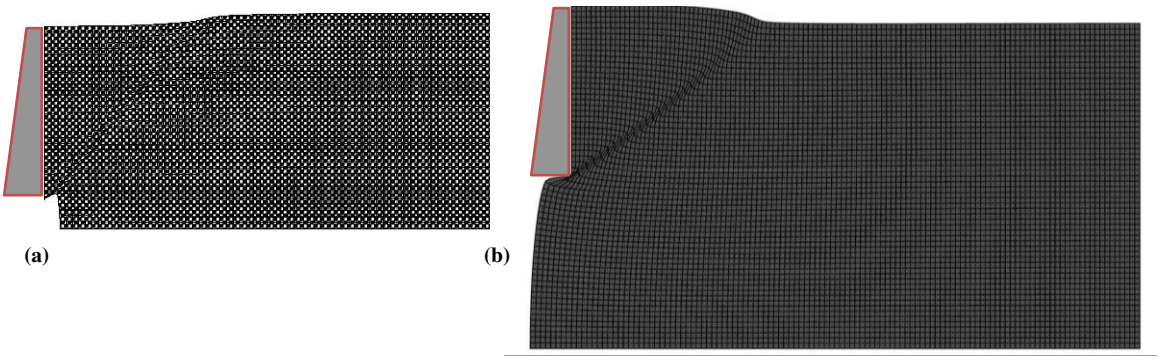

245 **Figure 3.** Typical mrearth2d models at failure for a) the active state (64 × 36 mesh) and b)
246 the passive state (120 × 60 mesh). Figures showing a 30-element, perfectly smooth, translating
247 wall (wall displacement not in scale).

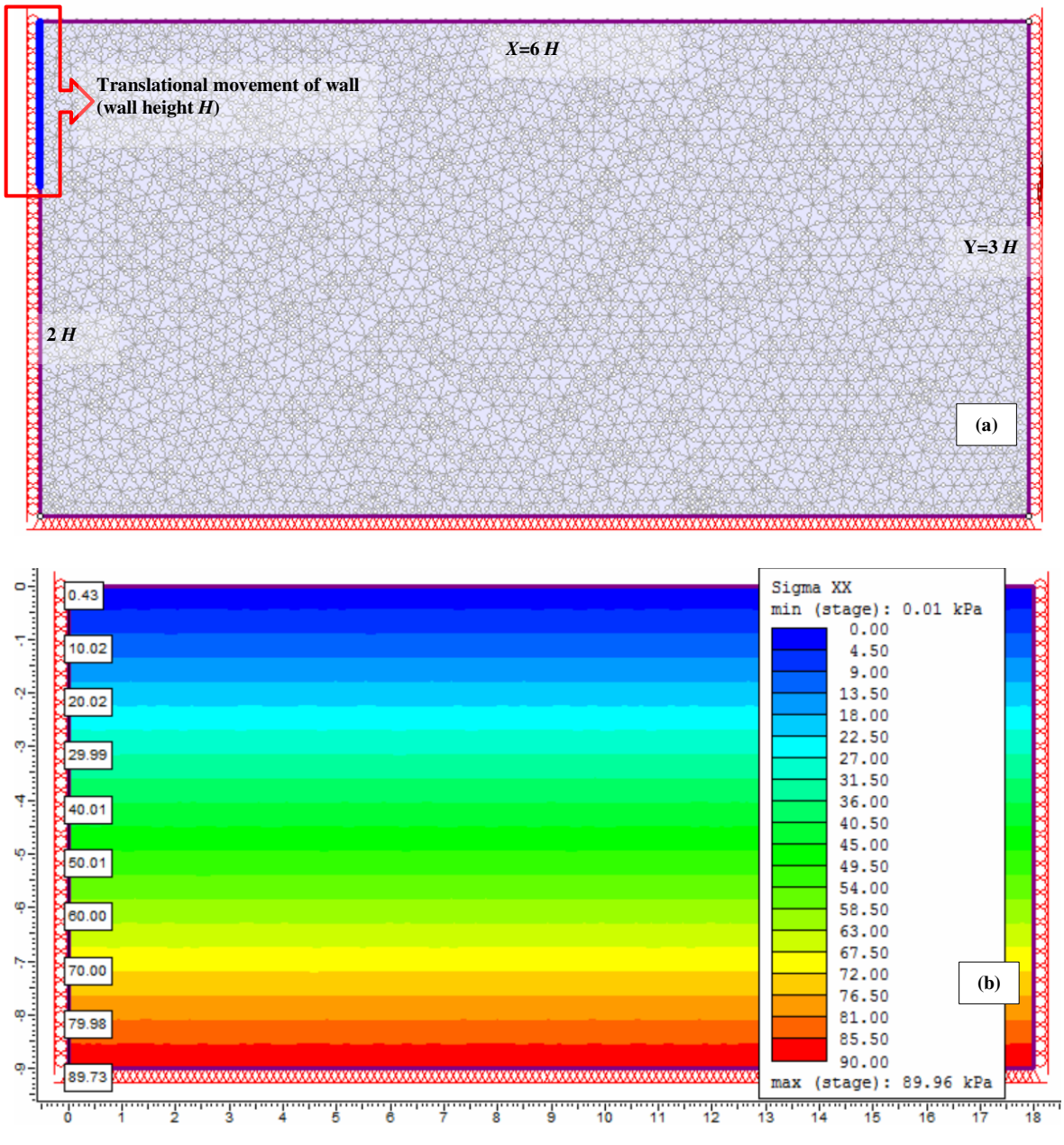

Figure 4. a) The general RocScience's RS2 model used for the passive state problems, b) Checking the initial horizontal stresses statically derived from RS2 against Jaky's at-rest earth pressure (φ=30°, γ=20 kN/m^3).

2.3.2 Validating the generalized coefficient of earth pressure at-rest through the initial stresses in finite element analysis

Table 1 presents thirteen example walls retaining cohesionless soils; cohesion was taken equal to zero for avoiding unlucky comparisons between an analytical method taking into account tension crack formation and a numerical analysis not allowing the mesh to break. The height of wall H, the friction angle of soil and the horizontal pseudo-static coefficient are given in columns c1.1-c1.3 respectively (other data not listed on the table are: $c' = 0\ kPa$, $\gamma = 20\ kN/m^3$, $k_v = 0$). These examples were solved with the mrearth2d program two times. First, in the usual way, calculating the initial stresses using Jaky's $Ko = 1 - \sin\varphi'$ static coefficient of earth pressure at-rest (i.e. use of $k_h = k_v = 0$ in Equation 1), before solving each example with the respective k_h value (and $k_v = 0$). The second time, the same examples were solved anew with two alterations: the initial stresses were calculated using Equation 1 with the k_h values of Table 1 (and $k_v = 0$) and the models were run statically (i.e. $k_h = k_v = 0$). The two groups of resultant active earth pressure force values P_{AE} are summarized in columns c.1.4 and c.1.5 of Table 1 respectively. As shown, the two procedures led to absolutely similar results, advocating for the validity of the K_{OE} expression of Equation 1. For convenience, readers may focus on the relative difference (*RD*) values given in column c.1.6, which are limited to a few units with an average of just 2.3%. The mrearth2d program gives directly the resultant active earth pressure force. The K_{OE} values are given in column c1.7.

2.3.3 Examining the validity of the active earth pressure coefficients: case of cohesionless soils

A subsequent step is the comparison of the numerical P_{AE} values (column c1.4) with the respective analytical ones. In this respect, the analytical active earth pressures by the proposed method were calculated using Equations 2 and 3, while the resultant P_{AE} values by the chart area bounded by the earth pressure distribution along the wall and the z-axis (mathematical integration of a best fit polynomial curve of 3rd degree; recall Equation 14). The analytical P_{AE} values and the respective *RD* values are given in columns c1.9 and c1.10 of Table 1 respectively. As shown, the derived *RD* values belong again in the sphere of the common modelling error, with an average value of just -2.6%.

The analytical methods included in EN1998-5:2004 and the draft standard prEN1998-5:2022, were evaluated also against the respective numerical results. These P_{AE} values are given in columns c1.11 and c1.13 while the relative difference values as for mearth2d (c1.4), in columns c1.12 and c1.14 respectively. K_{AE} coefficients by the proposed method are also given (c1.8). The comparison of the results confirms the conclusion drawn in the various contemporary studies referenced in Section 2.2, that the M-O method is very conservative in evaluating the active state of soil (see columns c1.11 and c1.12 in Table 1). On the other hand, the prEN1998-5:2020 method appears to be even more conservative (see columns c1.13 and c1.14). It is worth mentioning that, for the examples considered herein, the absolute maximum and average *RD* values found were 50.3% and 25.8% respectively for EN1998-5:2004 and as high as 105% and 44.7% for prEN1998-5:2022. Apparently, these are not acceptable *RD* values. The numerical values of column c1.4 were used as reference point for calculating all relative differences in Table 1.

2.3.4 Examining the validity of the passive earth pressure coefficients: case of cohesionless soils

For evaluating the validity of the generalized coefficient of passive earth pressure, it was considered fair the same 13 example walls to be used. The only difference in modelling the passive state with the mrearth2d program was the direction of movement of the wall (translational movement, towards soil). The results are shown in column c2.1 of Table 2, while the respective analytical values derived using the proposed method are listed in column c2.5 (the K_{PE} values derived from the proposed method are given in column c2.4). Comparing these results, the *RD* values were found to be very small with an average value as low as -0.1% (column c2.6). Application of RS2 (column c2.2) showed a consistent behavior with average *RD* value against mrearth2d equal to -8% (c2.3). It is noted that the RS2 values in column c2.2 correspond to $2\Delta x_{max}$ and not the desirable Δx_{max}; however, this is something that it is discussed later.

Regarding prEN1998-5:2022, application of this norm revealed quite similar results (though slightly conservative, with average *RD* equal to 13.1%; see c2.9), while the EN1998-5:2004 norm returned non-conservative results with maximum and average *RD* values, 46.2% and 23.9% respectively (c2.11). Finally, the proposed method was also compared against RS2; the results are shown in column c2.7, showing an average *RD* value 9.9%.

2.3.5 Examining the validity of the passive earth pressure coefficients: case of cohesive-frictional soils

So far, the same 13 examples were used in all comparisons, just for the sake of uniformity. However, for the passive state there is no excuse for avoiding the use of soil's cohesion. In this respect, Example No 3 (recall Table 1) was used as the basis for producing nine additional examples denoted by numbers 3.1 to 3.9 in Table 3. In the examples No 3.0 (i.e., example No 3) to No 3.4, cohesion ranges from 0 kPa to 40 kPa with 10 kPa interval, while k_h was kept equal to 0.2. In the next five examples (No 3.5 to No 3.9) the only difference is the k_h value which was increased to 0.3. It is important to be noted that EN1998-5:2004 has no provision for taking into account soil's cohesion; in this respect the earth pressures were calculated using the prEN1998-5:2022 expression for *c'- φ΄* soils (recall Equation 12); these results have been marked in Table 3 with star (*). According to Table 3, both the proposed and EN1998-5:2004 methods appear to perform satisfactorily, while prEN1998-5:2022 is rather conservative with an average *RD* value -19.1%. The mrearth2d results were used as reference point for calculating all *RD* values in Table 3. However, the authors would like to emphasize that any agreement of EN1998-5:2004 results with the numerical ones is only coincidental. In this respect, several new examples are given in Table 4. Table 4 is divided into three parts, with the last one referring to examples where the two Eurocode 8-5 methods deal with their negative root problem. From these examples, it is inferred that extreme relative difference values may easily be observed and indeed, on the unsafe side; the proposed method was used as reference point for calculating the *RD* values in Table 4.

337 **Table 1.** Comparison examples for the active state case of cohesionless soils (data shown in

338 columns c1.1 to c1.3; $c' = 0\ kPa,\ \gamma = 20\ kN/m^3$, $k_v = 0$ for all cases)

S/N	Data			mrearth2d			Proposed method				EN1998-5: 2004		prEN1998-5: 2022	
				$\{K_O,\ k_h\}$	$\{K_{OE},\ k_h=0\}$									
	H	φ'	k_h	$P_{AE,1}$	P_{AE}	RD_1	K_{OE}	K_{AE}	P_{AE}	RD_1	P_{AE}	RD_1	P_{AE}	RD_1
	(m)	(deg)	-	(kN)	(kN)	(%)	-	-	(kN)	(%)	(kN)	(%)	(kN)	(%)
	c1.1	c1.2	c1.3	c1.4	c1.5	c1.6	c1.7	c1.8	c1.9	c1.10	c1.11	c1.12	c1.13	c1.14
1	3	40	0.2	27.8	24.1	13.3	0.417	0.290	26.1	6.1	29.6	-6.5	31.5	-13.3
2	3	35	0.2	32.1	29.5	8.1	0.486	0.347	31.2	2.8	35.6	-10.9	37.8	-17.8
3	3	25	0.2	44.8	42.4	5.4	0.631	0.482	43.3	3.3	50.8	-13.4	53.7	-19.9
4	3	35	0.4	38.5	34.6	10.1	0.546	0.423	38.1	1.0	52.3	-35.8	64.7	-68.1
5	3	35	0.3	33.9	32.3	4.7	0.516	0.385	34.6	-2.1	43.0	-26.8	48.8	-44.0
6	3	35	0.1	29.6	27.1	8.4	0.456	0.309	27.8	6.1	29.5	0.3	30.0	-1.4
7	2	25	0.2	20.2	19.1	5.4	0.631	0.482	19.3	4.5	22.6	-11.9	23.9	-18.3
8	1	30	0.3	4.5	4.3	4.4	0.587	0.449	4.5	0.0	5.7	-26.7	6.4	-42.2
9	1.5	30	0.3	10.2	9.6	5.9	0.587	0.449	10.1	1.0	12.8	-25.5	14.5	-42.2
10	2	30	0.3	18.0	17.1	5.0	0.587	0.449	18.0	0.0	22.8	-26.7	25.7	-42.8
11	2.5	30	0.3	28.4	26.9	5.3	0.587	0.449	28.1	1.1	35.6	-25.4	40.2	-41.5
12	3	30	0.3	42.3	38.4	9.2	0.587	0.449	40.4	4.5	51.2	-21.0	57.9	-36.9
13	1.5	25	0.3	12.2	11.4	6.6	0.658	0.519	11.7	4.1	15.3	-25.4	17.4	-42.6
Average						7.1				2.5		-19.7		-33.1

339
340
341

342 **Table 2.** Comparison examples for the passive state case of cohesionless soils (data as indi-
343 cated in Table 1)

S/N	mrearth2d	RS2 ($2\Delta x_{max}$)		Proposed method				prEN1998-5:2022		EN1998-5:2004	
	$P_{PE,1}$ (kN)	$P_{PE,2}$ (kN)	RD_1 (%)	K_{PE} -	P_{PE} (kN)	RD_1 (%)	RD_2 (%)	P_{PE} (kN)	RD_1 (%)	P_{PE} (kN)	RD_1 (%)
	c2.1	c2.2	c2.3	c2.4	c2.5	c2.6	c2.7	c2.8	c2.9	c2.10	c2.11
1	286	294.9	-3.1	3.055	275	3.8	6.7	372.3	-30.2	373.7	-30.7
2	237.7	255.1	-7.3	2.657	239.1	-0.6	6.3	294.1	-23.7	295.7	-24.4
3	171.2	181.7	-6.1	2.004	180.7	-5.5	0.6	188.6	-10.2	190.7	-11.4
4	173.6	167.4	3.6	1.623	146.1	15.8	12.7	247.5	-42.6	253.8	-46.2
5	201.8	222.3	-10.2	2.14	192.6	4.6	13.4	272.2	-34.9	275.7	-36.6
6	260.2	290.5	-11.6	3.173	285.6	-9.8	1.7	314	-20.7	314.4	-20.8
7	76.3	87	-14	2.004	80.2	-5.1	7.8	83.8	-9.8	84.8	-11.1
8	20.2	21.1	-4.5	1.961	19.6	3.0	7.1	23.7	-17.3	24.2	-19.8
9	44.2	49.8	-12.7	1.961	44.1	0.2	11.4	53.7	-21.5	54.4	-23.1
10	79.3	88.5	-11.6	1.961	78.4	1.1	11.4	94.9	-19.7	96.7	-21.9
11	123.2	131.2	-6.5	1.961	122.6	0.5	6.6	148.2	-20.3	151.1	-22.6
12	174.6	190.2	-8.9	1.961	176.5	-1.1	7.2	213.5	-22.3	217.6	-24.6
13	37.8	42.2	-11.6	1.775	39.9	-5.6	5.5	41.7	-10.3	43	-13.8
Average			-8.0			0.1	7.6		-21.8		-23.6

344

345

346 **Table 3.** Comparison examples for the passive state case of cohesive-frictional soils ($H =$

347 $3\,m,\ \gamma = 20\ kN/m^3,\ k_v = 0$ for all cases).

S/N	Data		mrearth2d	Proposed method		prEN1998-5:2022		EN1998-5:2004	
	c'	k_h	$P_{PE,1}$	P_{PE}	RD_1	P_{PE}	RD_1	P_{PE}	RD_1
	(kPa)	-	(kN)	(kN)	(%)	(kN)	(%)	(kN)	(%)
	c3.1	c3.2	c3.3	c3.4	c3.5	c3.6	c3.7	c3.8	c3.9
3.0	0	0.2	172.5	180.7	-4.8	188.6	-9.3	190.7	-10.6
3.1	10		262.7	263.7	-0.4	275.4	-4.8	*278.1	-5.9
3.2	20		348.8	340.2	2.5	362.4	-3.9	*365.4	-4.8
3.3	30		439.4	425.6	3.1	449.1	-2.2	*452.8	-3.0
3.4	40		536.2	513	4.3	536	0.0	*540.1	-0.7
3.5	0	0.3	150.7	159.7	-6.0	166.8	-10.7	171.9	-14.1
3.6	10		241	227.1	5.8	248.5	-3.1	*254.8	-5.7
3.7	20		336.5	302.5	10.1	330.1	1.9	*337.7	-0.4
3.8	30		421	382.7	9.1	411.8	2.2	*420.6	0.1
3.9	40		509.8	466.2	8.6	493.5	3.2	*503.5	1.2
Average					-3.2		-2.7		4.0

348 * Use of prEN1998-5:2022 expression for *c'- φ'* soils (recall Equation 12)

349

350 **Table 4.** Additional examples for cohesive-frictional soils.

Data (γ = 20 kN/m^3; H = 3 m)	c' (kPa)	Proposed method $P_{PE,1}$ (kN)	EN1998-5:2004 P_{PE} (kN)	EN1998-5:2004 * P_{PE} (kN)	prEN1998-5:2022 P_{PE} (kN)	EN1998-5:2004 RD_1 (%)	EN1998-5:2004 * RD_1 (%)	prEN1998-5:2022 RD_1 (%)
c4.1	c4.2	c4.3	c4.4	c4.5	c4.6	c4.7	c4.8	c4.9
φ'= 35°	0	149.1	253.8	253.8	247.5	-70.2	-70.2	-66.0
k_h=0.4	20	273.4	253.8	455.3	446.4	7.2	-66.5	-63.3
	40	446.3	253.8	656.8	645.4	43.1	-47.2	-44.6
φ'= 40°	0	275.0	373.7	373.7	372.3	-35.9	-35.9	-35.4
k_h=0.2	20	479.8	373.7	618.2	616.5	22.1	-28.8	-28.5
	40	705.3	373.7	862.8	860.5	47.0	-22.3	-22.0
φ'= 10°	0	109.8	100.1	100.1	172.8	8.8	8.8	-57.4
k_h=0.4	20	214.4	100.1	226.5	339.1	53.3	-5.6	-58.2
**	40	338.5	100.1	353.1	505.4	70.4	-4.3	-49.3

351 * Use of prEN1998-5:2022 expression for *c'- φ'* soils (recall Equation 12)

352 ** EN1998-5:2004 and prEN1998-5:2022 dealing with their negative root problem.

2.4 Examining the validity through experimental results

2.4.1 Comparison against press-in cell measurement

This example was chosen because a single source [35] includes an in-situ earth pressure measurement with a GLÖTZL Baumeßtechnik press-in cell and all the necessary information for calculating the theoretical earth pressure at-rest coefficient with the proposed method. The testing material refers to an overconsolidated clay at Tiller (Trondheim Region, Norway), while the measurement was conducted quite recently (November 2016) by technical operators from Norwegian Geotechnical Institute (NGI). More specifically, the samples were taken from depth equal to 5 m, while the laboratory tests gave friction angle, cohesion, unit weight and over-consolidation ratio (OCR) equal to 32 degrees, 4.4 kPa, 18.5 kN/m^3 and 1.6 respectively. The measured in-situ horizontal stress with the earth pressure cell at depth 5 m led to an earth pressure at-rest coefficient equal to 0.56 ($K_{O,OC}$, overconsolidated coefficient of earth pressure at-rest). Calculating the same coefficient with the proposed analytical method, a value equal to 0.562 was obtained; the effect of overconsolidation of soil was taken into account through Mayne and Kulhawy's [36] equation $K_{O,OC} = K_{O,NC} OCR^{\sin\varphi'}$ ($K_{O,NC}$, coefficient of earth pressure at-rest for normally consolidated soils). It is mentioned that the calculated mobilized cohesion and friction angle at depth 5 m were c_m =2.66 kPa and φ_m =20.68^o respectively.

Ignoring cohesion, the calculated earth pressure at-rest coefficient would be 0.603, that is, by 7.7% higher compared to the measured value; apparently, a much higher relative error would be expected for greater cohesion values. This is very important as, ignoring cohesion e.g. in studying axially loaded piles, the error may be very high and indeed, on the unsafe side.

2.4.2 Comparison with contemporary centrifuge test results

2.4.2.1 Mikola and Sitar (2013)

The active earth pressure coefficients for seismic situation derived from the proposed method and by the methods included in EN19985-5:2004 and prEN1998-5:2022 are compared herein against contemporary centrifuge test results; these tests have been carried out at the facilities of the Center for Geotechnical Modeling of U.C. Davis (University of California, Davis) by Mikola and Sitar [21] from Berkley University of California. Centrifuge tests have the advantage of avoiding the limitations of the 1-g shaking table, whilst scaling laws can be accurately followed. The objective of this study was to evaluate the dynamic behavior of structures retaining granular, dry sand backfill.

Two Mikola and Sitar's experiments referring to the dynamic active earth pressure on cantilever displacing walls are presented, namely, the loma prieta sc and the kobe tak090. Dry medium-dense sand with relative density on the order of from 75% to 80% was used as backfill. The friction angle and the unit weight of the sand was φ'=35°, γ=16.6 kN/m³ (taken from [21, 26]. The loma prieta sc wall was tested for k_h=0.51 while the kobe tak090 for 0.61. The static earth pressure profiles measured by pressure cells on outside and inside of the loma prieta sc and the kobe tak090 walls are given in Figure 5. This normalized height versus normalized earth pressure (i.e., $\sigma_H/\gamma H = \sigma_A/\gamma H = K_A$) charts in Figure 5, is rather a validation of Rankine's theory for active earth pressure under controlled conditions (Rankine's active earth pressure coefficient for φ'=35° is equal to 0.271).

For dynamic conditions, Mikola and Sitar used the "interpreted dynamic earth pressure". In this respect, the area underneath the dynamic pressure distribution given by earth pressure

transducers was corrected based on overall load estimate by load cells and the corresponding linear pressure profiles were back calculated (the procedure is explained in detail in Mikola and Sitar [21]. The "interpreted earth pressures" are shown in Figure 6. The charts in Figure 6 are also in normalized form with normalized wall height as vertical axis and the $K_{AE} - K_A$ difference as horizontal axis (i.e $\Delta\sigma_{AE}/\gamma H = K_{AE} - K_A$). Mikola and Sitar's results are indicated on the two charts of Figure 6 with continues line with dots, while the respective results derived from the proposed method have been marked with green marker line; it is remarkable how analytical results validates the experimental ones and vice versa; for $z = H$, following the proposed method, $\Delta\sigma_{AE}/\gamma H = K_{AE} - K_A = 0.464 - 0.271 = 0.193$ for the loma prieta sc wall and $0.502 - 0.271 = 0.231$ for the kobe tak09 wall.

The results of application of EN1998-5:2004 (i.e. Mononobe-Okabe method), prEN1998-5:2022 and Seed and Whitman [37] methods are also shown on the same charts. The over-conservatism of EN1998-5:2004 and prEN1998-5:2022 methods is more than obvious. It is also noted that, the inverted triangle pressure distribution for the seismic increment of active earth pressure suggested by Seed and Whitman is rather far from reality. Seed and Whitman modified the M-O method separating the M-O seismic active pressure into two components, the active static component P_A and the seismic increment of active earth pressure ΔP_{AE}; the latter is applied at $2/3H$ above the base of the wall (i.e., inverted triangular pressure distribution).

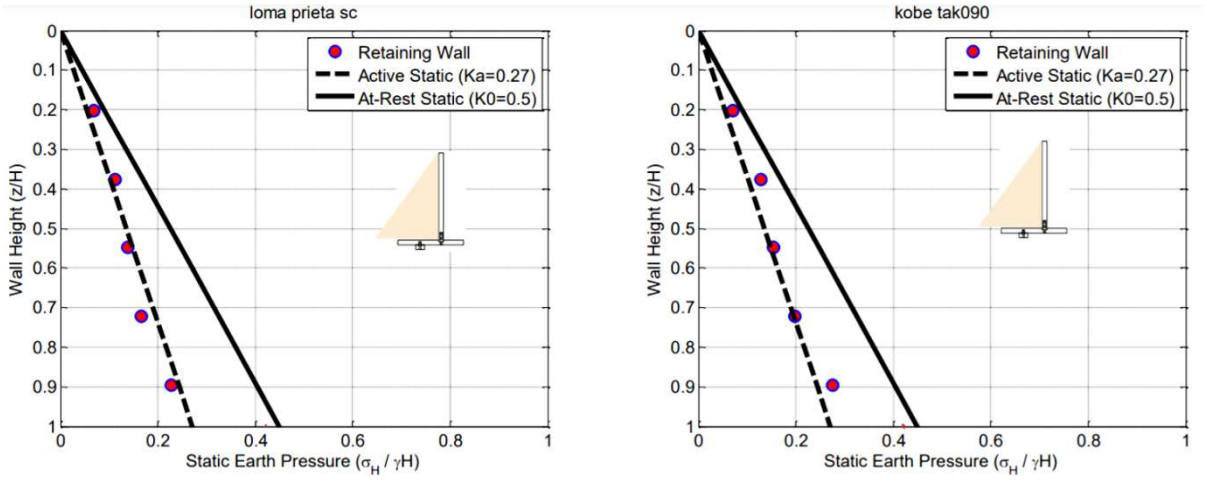

416

417 **Figure 5.** Mikola and Sitar's (2013) experimental values for the static case of loma prieta sc

418 and kobe tak090 tests.

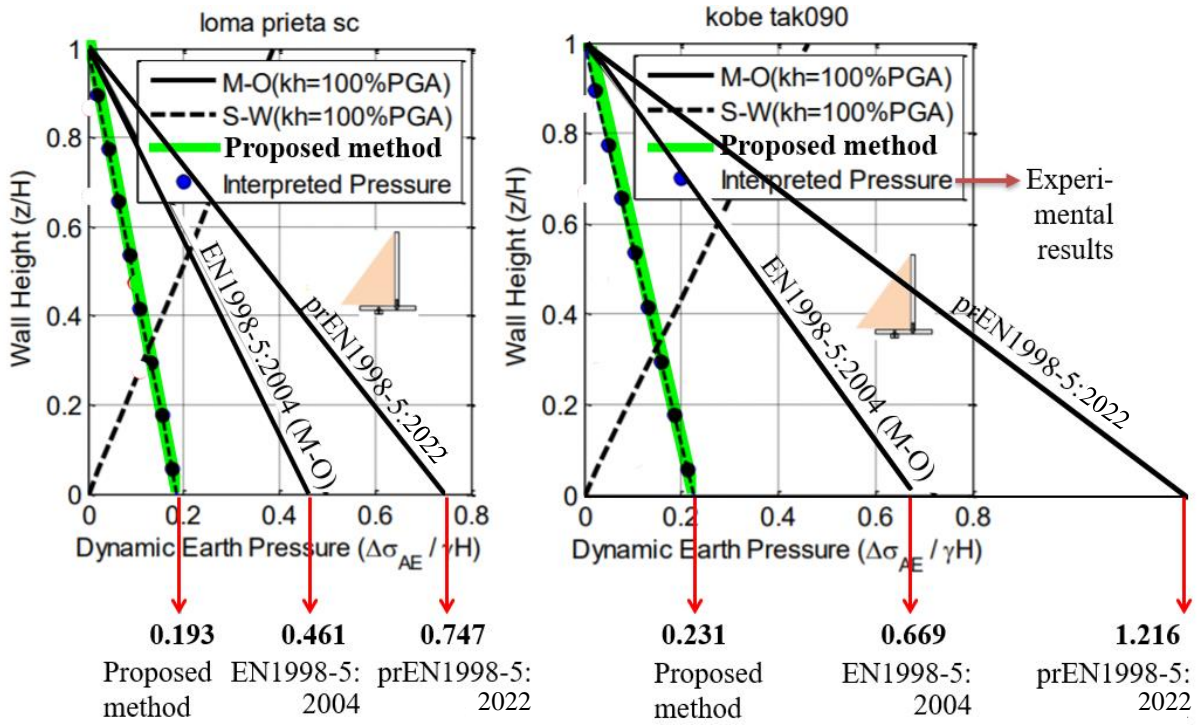

419

420 **Figure 6.** Comparison of Mikola and Sitar's experimental values for the seismic situation

421 case of loma prieta sc and kobe tak090 tests against the proposed, EN1998-5:2004, prEN1998-

422 5:2022, Seed and Whitman's methods.

423

2.4.2.2 Olson et al. [38]

Olson et al. [38] published centrifuge test results for evaluating limiting lateral earth pressures imposed on a large, stiff foundation. The soil was a loose, saturated, potentially liquefiable Nevada sand with saturated unit weight of 19.4 kN/m^3, corresponding to D_r= 35%. From direct shear tests and the angle of repose, Olson et al. selected an effective internal friction angle for the sand equal to 35°. Olson et al.'s total earth pressure experimental results for I-A3 test and the respective analytical results by the proposed method are presented together in Figure 7 (Olson et al.'s results for the I-A2 test are very similar to their I-A3 test). Input motions for Olson et al.'s centrifuge tests consisted of three low-amplitude cycles ($\pm 0.01g$) followed by 20 cycles of strong shaking ($\pm 0.2g$). The figure in question clearly shows very good agreement between the two methods for the passive state up to depth approximately 2.1 meters and for the active state for a depth up to 5.7m (for the active state, the linear analytical relationship intersects the vertical axis approximately one meter below the soil surface ($\Delta z = 1.0$ m), as it seems that the latter subsided significantly during the active failure). From z=2.1 m to 10 m (lower end of the caisson) for the "passive side" of the problem, the experimental results follow a different earth pressure distribution, which match perfectly with the earth pressure at-rest distribution derived from the proposed method. The most possible explanation is that the displacement was insufficient to trigger the passive failure along the entire height of the caisson. Unfortunately, Olson et al. have not provided the elastic parameters of soil, something that would allow the back-calculation of Δx_{max} at point-level (use of Equation 4) and more importantly, the mid-height Δx_{max} (i.e., $\Delta x_{max}(z = H/2)$). In this respect, setting the first derivative of Equation 4 as for z equal to zero and solving as for the same parameter, Equation 4 has

maximum at $H/2$. The latter means that if the wall moves towards the soil by $\Delta x = \Delta x_{max}(z = H/2)$ the soil is at the passive state along the whole height of the wall (it is reminded that Δx_{max} is different in the two failure states, active and passive; recall Equation 4). Consequently, if $\Delta x < \Delta x_{max}(z = H/2)$, three zones seem to exist simultaneously in the retained soil. An upper and a lower zone, which are both passive state zones and an intermediate zone, where the soil has not failed yet because of insufficient displacement. However, although theoretically the lower zone is at a passive failure state, this will rather adopt the state of the intermediate zone which is immediately above it; otherwise, the failure surface would be discontinuous. This behavior is shown in the "passive side" of the experimental data of Figure 7. Based on Equation 4 and the two distributions derived from the proposed method (the passive and the at-rest distribution intersecting at $z \approx$2.1 m), an additional $1 - \Delta x_{max}(2.1m)/\Delta x_{max}(H/2)$= 17.1% displacement was necessary so that the passive state to fully develop (in this respect, the knowledge of the elastic parameters of soil was not necessary).

For the "active side" of the problem, as shown, a different earth pressure distribution (other than the active one) describes the soil state from z=5.7 m and below. The state that effectively describes this lower zone is the liquefaction state (K=1). In this respect, it seems that liquefaction first occurred at a depth of (approximately) 5.7 m and propagated downward gradually; this was rather an expected behavior for a saturated, potentially liquefiable sand with D_r= 35%, besides, the existence of a liquefaction zone below a non-liquefaction zone is a typical situation [39, 40].

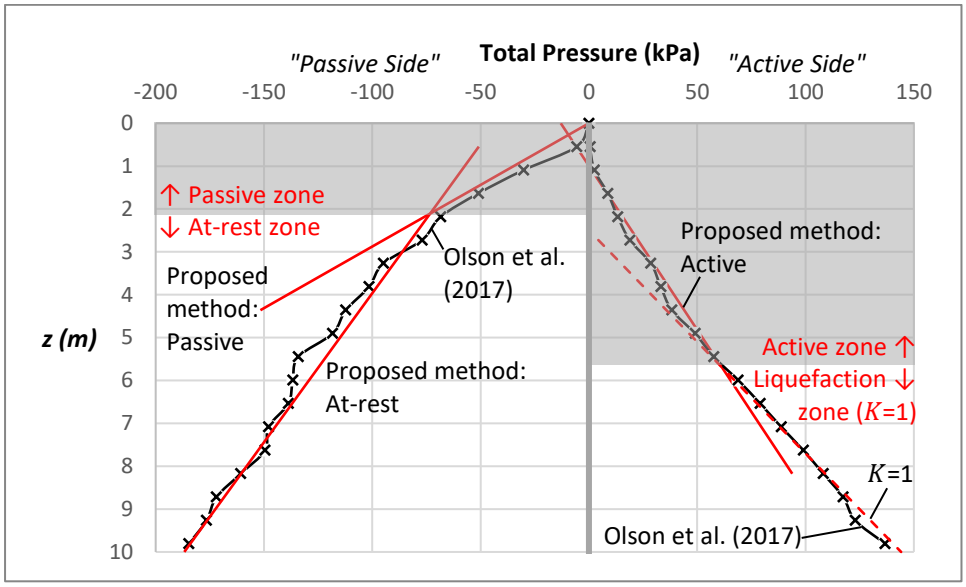

Figure 7. Comparison chart comparing Olson et al.'s experimental results against the respective ones obtained by the proposed method (negative pressure values simply indicate the "passive side" of the problem). Proposed method: $K_{AE} = 0.347$, $K_{OE} = 0.486$ and K_{PE} =2.657.

Finally, both from the back-calculation and the very form of Olson et al.'s experimental results, it is concluded that all water pressures acted on the caisson were hydrostatic. However, the computations present a peculiarity. Although in the "passive side" the coefficient of earth pressure changes from K_{PE} =2.657 to $K_{OE} = 0.486$ at depth 2.1 m and from K_{AE} =0.347 to $K_{Liq} = 1$ at depth 5.7 m in the "active side", the material is still the same homogenous sand. Thus, the earth pressures are calculated as in the case of a common homogenous soil, where the earth pressure at depth $z + dz$ derives from the summation of the earth pressure at depth z and the earth pressure increment corresponding to dz $(e.g. K_1\gamma z + K_1\gamma dz = K_1\gamma(z + dz))$; the only difference is that there is a different K value along dz (i.e. $K_1\gamma z + K_2\gamma dz$). The computations for the total pressures on the wall for the "passive side" have as follows:

- z_1=2.1 m: $\sigma_{PS,2.1m} = K_{PE}\gamma' z_1 + \gamma_w z_1 = 2.657 \cdot 9.4 \cdot 2.1 + 9.81 \cdot 2.1 = 73.1$ kPa
- z_2=10 m: $\sigma_{PS,10m} = \sigma_{PS,2.1m} + K_{OE}\gamma'(z_2 - z_1) + \gamma_w(z_2 - z_1) =$

$$= 73.1 + 0.486 \cdot 9.4 \cdot 7.9 + 9.81 \cdot 7.9 = 186.7 \text{ kPa}$$

while the computations for the "active side" are:

- z_3=5.7* m: $\sigma_{AS,5.7m} = K_{AE}\gamma'(z_3 - \Delta z) + \gamma_w(z_3 - \Delta z) =$

$$= 0.347 \cdot 9.4 \cdot (5.7 - 1.0) + 9.81 \cdot (5.7 - 1.0) = 61.4 \text{ kPa}$$

- z_4=10* m: $\sigma_{AS,10m} = \sigma_{AS,5.7m} + K_{Liq}\gamma'(z_4 - z_3) + \gamma_w(z_4 - z_3) =$

$$= 61.4 + 1 \cdot 9.4 \cdot 4.3 + 9.81 \cdot 4.3 = 144.0 \text{ kPa}$$

The star symbol (*) have been used for reminding of the subsidence of the free surface on the "active side of the problem" (i.e., actual z_3=4.7 m, while actual z_4=9.0 m).

The resultant earth pressure forces are summarized in Table 5. As shown, the two Eurocode 8-5 methods largely fail to predict the earth pressure force on the "passive side" (RD>80%), while the active earth pressure forces are similar to Olson's experimental results and the results obtained by the proposed method, just because the two Eurocode 8-5 coefficients (K_{AE}=0.396 and 0.420) are between the active and the at-rest coefficients (K_{AE}=0.347 and K_{OE}=0.486 respectively). On the other hand, the proposed method effectively predicted the total earth pressures on both the active and the passive side of the problem.

Table 5. Comparison or Olson et al' experimental total earth pressure distributions with the respective ones obtained using the proposed method as well as the methods included in EN1998-5:2004 and, prEN1998-5:2022.

Method	K_{OE}	K_{AE}	K_{PE}	P_{AE} (kPa)[1]	$P_{AE} + P_{Liq}$ (kPa)[1]	P_{PE} (kPa)[2]	$P_{PE} + P_{OE}$ (kPa)[2]
Olson et al. (2017)	-	-	-	-	546.7	-	1072.5
Proposed method	0.486	0.347	2.657	-	566.4	-	1078.3
EN1998-5:2004	-	0.396	3.286	654.6	-	1988.1	-
prEN1998-5:2022	-	0.420	3.268	665.6	-	1980.2	-

[1] "Active side": Values referring to depth from 1 m (due to soil subsidence) to 9.81 m (deepest sensor)

[2] "Passive side": Values referring to depth from zero to 9.81 m (deepest sensor)

3 Validation of the mobilized shear strength formulae

3.1 Calculating the earth pressure at-rest through the active earth pressure coefficient

The derivation of the earth pressure at-rest by the active earth pressure coefficient has been foreseen by the U.S. Army Corps of Engineers [12] assuming an average Strength Mobilization Factor (SMF) along Coulomb's failure surface equal to 2/3 (applicable to $\tan\varphi'$, i.e. $2/3\tan\varphi'$). For example, for φ' equal to 30, Jaky's coefficient gives:

$$K_O = 1 - \sin\varphi' = 1 - \sin(30°) = 0.500 \tag{16}$$

Reducing, now, the shear strength along the failure surface following USACE's empirical rule (i.e., $\varphi_m = \arctan[(2/3)\tan\varphi' = 21.05°$) and using this reduced value in Rankine's active earth pressure coefficient, the coefficient of earth pressure at-rest would be:

$$K_O = K_A(\varphi_m = 21.05°) = \frac{1-\sin\varphi_m}{1+\sin\varphi_m} = \frac{1-\sin(21.05°)}{1+\sin(21.05°)} = 0.471 \tag{17}$$

This value is quite close to Jaky's 0.5 value, but using the proposed method, the calculations are exact. A more complete example is given, considering, in addition to the friction angle of soil, its cohesion and unit weight, the depth of interest and the two seismic coefficients (vertical and horizontal). More specifically, for c'= 20 kPa, φ'= 30 degrees, γ= 18 kN/m^3, k_h= 0.3, k_v = 0.15 and z= 2 m, following the proposed method, the derived mobilized shear strength values are c_m=6.06 kPa and φ_m=9.92°, while the generalized earth pressure at-rest coefficient of Equation 1 gives

$$K_{OE} = (1 - \sin\varphi')\left(1 + \frac{k_h}{1-k_v}\tan\varphi'\right) - \frac{1}{1-k_v}\frac{2c_m}{\gamma z}\cdot\tan\left(45^o - \frac{\varphi'}{2}\right) =$$

$$= \left(1-\sin(30°)\right)\left(1+\frac{0.3}{1-0.15}\cdot\tan(30°)\right)-\frac{1}{1-0.15}\cdot\frac{2\cdot 6.06}{18\cdot 2}\cdot\tan\left(45-\frac{30°}{2}\right)=0.373 \quad (18)$$

Now, setting k_h=0 and feeding Equation 2 with the above-mentioned mobilized shear strength values (i.e. c_m=6.06 kPa and $\varphi' = \varphi_m$=9.92°), γ=18 kN/m^3 and k_v=0.15, this gives

$$K_{OE,\text{from } Eq.2} = \frac{1-\sin\varphi'}{1+\sin\varphi'}\left(1+2\cdot\frac{k_h}{1-k_v}\cdot\tan\varphi'\right)-\frac{1}{1-k_v}\frac{2c_m}{\gamma z}\tan\left(45^o-\frac{\varphi'}{2}\right)=$$

$$= \frac{1-\sin(9.92°)}{1+\sin(9.92°)}\left(1+2\frac{0}{1-0.15}\tan(9.92°)\right)-\frac{1}{1-0.15}\cdot\frac{2\cdot 6.06}{18\cdot 2}\tan\left(45^o-\frac{9.92°}{2}\right)=0.373 \quad (19)$$

that is, the very same value. k_v in Equation 19 was kept equal to its initial value, because the vertical seismic excitation simply affects the (unit) weight of soil in the rather very common $(1-k_v)\gamma$ way.

3.2 Numerical validation

3.2.1 Replacing the $\{\varphi', k_h\}$ values with their $\{\varphi_m, k_h=0\}$ equivalent ones in passive earth pressure problems

The finding presented in Section 3.1 implies that a pseudo-static earth retention problem can be replaced by a respective static analysis, just substituting φ' of the original problem with φ_m of the equivalent problem (the seismic information is already included in φ_m). In addition to the previous solutions presented in Table 2 (see the automatically derived mearth2d values in column c2.1 and the RS2 values for $2\Delta x_{max}$ in c2.2, both for $\{\varphi', k_h\}$), the same 13 passive state examples were solved again with mrearth2d for $\{\varphi_m, k_h=0\}$ (column c6.6 in Table 6), as well as with RS2 for $\{\varphi_m, k_h=0, \Delta x_{max}\}$ and $\{\varphi_m, k_h=0, 2\Delta x_{max}\}$ (columns c6.10 and c6.12

544 respectively). All numerical P_{PE} values are compared against those produced using the pro-
545 posed method (column c2.5). The analytically derived φ_m and Δx_{max} values are also given in
546 the same table (columns c6.2 and c6.3 respectively). All results, including the *RD* values, have
547 been aggregated in Table 6. The most interesting observation, however, is not the small *RD*
548 values when the mobilized shear strength of soil is used, but the more stable finite element
549 results, with the average *RD* values to be reduced from -0.5% to 0.2% and from -8.4% to 0.1%
550 for mrearth2d and RS2 respectively (the RS2 values refer to $2\Delta x_{max}$). Another interesting
551 observation is that the RS2 values for Δx_{max} and $2\Delta x_{max}$ are very similar; however, this is
552 discussed in the section devoted to Δx_{max}.

553 **3.2.2 Replacing the $\{c', \varphi', k_h\}$ values with the mid-height $\{c_m, \varphi_m\}$ ones and k_h=0 in**
554 **passive earth pressure problems**

555 For cohesive soils, c_m and φ_m depend on depth and thus, the equivalent models have to be
556 produced for shear strength values varying with depth (*SMF* varying with depth). For example,
557 for the Example 3.3 of Table 7, the SMF factor is equal to 1.000, 0.919, 0.876, 0.851, 0.835,
558 0.823 and 0.815 for z =0 to 3 m with 0.5 m interval ($c_m = c \cdot SMF$ and $\tan\varphi_m = \tan\varphi' \cdot$
559 SMF). Thus, for convenience the authors did something different. For all examples of Table 3,
560 the authors calculated the mid-height $\{c_m, \varphi_m\}$ values and then the mrearth2d and RS2 models
561 were run statically with these values. The average relative difference values obtained with
562 mrearth2d and RS2 was as small as 2.7% and 3.0% respectively (see columns c7.10 and c7.12);
563 all new P_{PE} values were compared against the values derived from the proposed method, re-
564 peated in column c3.4 of Table 7).
565

566 **Table 6.** Comparison table for the case of replacing the $\{\varphi', k_h\}$ values with their $\{\varphi_m,$

567 $k_h=0\}$ equivalent ones in passive earth pressure problems.

S/N	Proposed method			mrearth2d (φ', k_h, automatic)		mrearth2d (φ_m, k_h=0, automatic)		RS2* (φ', k_h, $2\Delta x_{max}$)		RS2* (φ_m, k_h=0, Δx_{max})		RS2* (φ_m, k_h=0, $2\Delta x_{max}$)	
	$P_{PE,1}$ (kN)	φ_m (°)	Δx_{max} (mm)	P_{PE} (kN)	RD_1 (%)	P_{PE} (kN)	RD_1 (%)	P_{PE} (kN)	RD_1 (%)	P_{PE} (kN)	RD_1 (%)	P_{PE} (kN)	RD_1 (%)
	c2.5	c6.2	c6.3	c2.1	c6.5	c6.6	c6.7	c2.2	c6.9	c6.10	c6.11	c6.12	c6.13
1	275.0	30.45	28.6	286.0	-4.0	275.4	-0.1	294.9	-7.2	245.0	9.6	257.5	6.3
2	239.1	26.94	23.6	237.7	0.6	239.3	-0.1	255.1	-6.7	213.5	7.2	229.4	3.3
3	180.7	19.53	14.9	171.2	5.3	180.5	0.1	181.7	-0.6	171.5	3.8	175.1	3.2
4	146.1	13.74	11.7	173.6	-18.8	146.1	0.0	167.4	-14.6	140.4	3.4	139.8	4.9
5	192.6	21.29	17.6	201.8	-4.8	192.7	-0.1	222.3	-15.4	180.0	4.2	186.4	3.3
6	285.6	31.38	29.5	260.2	8.9	286	-0.1	290.5	-1.7	254.9	16.6	265.3	7.0
7	80.2	19.53	6.6	76.3	4.9	79.4	1.0	87.0	-8.5	80.6	-1.9	86.4	-8.5
8	19.6	18.94	1.7	20.2	-3.1	19.6	0.0	21.1	-7.7	18.5	3.6	19.1	2.6
9	44.1	18.94	3.7	44.2	-0.2	43.9	0.5	49.8	-12.9	43.7	-1.8	47.7	-8.8
10	78.4	18.94	6.6	79.3	-1.1	78.0	0.5	88.5	-12.9	77.8	-2.0	84.7	-8.9
11	122.6	18.94	10.4	123.2	-0.5	121.5	0.9	131.2	-7.0	115.1	3.8	119.1	3.1
12	176.5	18.94	14.9	174.6	1.1	176.6	-0.1	190.2	-7.8	165.7	3.7	171.4	3.1
13	39.9	16.21	3.0	37.8	5.3	39.9	0.0	42.2	-5.8	40.8	-2.8	44.7	-9.0
Average					-0.5		0.2		-8.4		3.6		0.1

568

569

570 **Table 7.** Comparison table for the case of replacing the $\{c', \varphi', k_h\}$ values with the mid-
571 height $\{c_m, \varphi_m\}$ ones and k_h=0 in passive earth pressure problems.

S/N	DATA		Proposed method	mrearth2d (automatic)		Proposed method			mrearth2d (c_m,φ_m, k_h=0)		RS2 for Δx_{max} (c_m, φ_m, k_h=0)	
	c'	k_h	$P_{PE,1}$	P_{PE}	RD_1	c_m	φ_m	Δx_{max}	P_{PE}	RD_1	P_{PE}	RD_1
	(kPa)	-	(kN)	(kN)	(%)	(kPa)	(°)	(mm)	(kN)	(%)	(kN)	(%)
	c3.1	c3.2	c3.4	c3.3	c7.5	c7.6	c7.7	c7.8	c7.9	c7.10	c7.11	c7.12
3.0	0	0.2	180.7	172.5	4.5	0.0	19.5	14.9	177.8	1.6	175.9	2.7
3.1	10		263.7	262.7	0.4	8.0	20.4	25.9	250.8	4.9	252.9	4.1
3.2	20		340.2	348.8	-2.5	16.6	21.1	36.9	329.0	3.3	331.9	2.4
3.3	30		425.6	439.4	-3.2	25.5	21.6	47.9	409.1	3.9	411.0	3.4
3.4	40		513.0	536.2	-4.5	34.8	22.1	58.9	500.2	2.5	497.5	3.0
3.5	0	0.3	159.7	150.7	5.6	0.0	16.2	12.1	158.9	0.5	155.8	2.4
3.6	10		227.1	241.0	-6.1	6.8	17.6	21.5	222.2	2.2	221.3	2.6
3.7	20		302.5	336.5	-11.2	14.5	18.7	31.4	293.9	2.8	293.5	3.0
3.8	30		382.7	421.0	-10.0	22.9	19.6	41.7	371.8	2.8	370.0	3.3
3.9	40		466.2	509.8	-9.4	31.7	20.3	52.1	453.2	2.8	450.4	3.4
			Average		-3.6					2.7		3.0

572 ## 4 Validation of the analytical expression for Δx_{max}

573 ### 4.1 Validating Δx_{max} for the active failure state

574 Another point needing validation is the required displacement of the wall Δx_{max} for the
575 mobilization of the active state of soil, which is given by Equation 4. The same 13 examples
576 were solved again with the mrearth2d program but this time asking from the program to return
577 the P_{AE} value when the wall has been translated by the mid-height Δx_{max}. The results are
578 summarized in Table 8; the calculated Δx_{max} values are given in column c8.2. It is reminded
579 that the mrearth2d P_{AE} values given in column c.1.4 of Table 8 have been derived automatically
580 by the program, that is, without having to a-priory set the wall displacement. Again, the relative
581 difference values obtained were very small, with an average just -3.2% (column c.8.4).

582 **Table 8.** Validating Δx_{max} for the active failure state (case of purely frictional soils).

S/N	mrearth2d (automatic)	Proposed method	mrearth2d (for Δx_{max})	
	$P_{AE,1}$ (kN)	Δx_{max} (mm)	P_{AE} (kN)	RD_1 (%)
	c1.4	c8.2	c8.3	c8.4
1	27.8	1.4	29.3	-5.4
2	32.1	1.5	33.2	-3.4
3	44.8	1.6	46.1	-2.9
4	38.5	1.3	38.9	-1.0
5	33.9	1.4	36.3	-7.1
6	29.6	1.6	30.8	-4.1
7	20.2	0.7	20.5	-1.5
8	4.5	0.2	4.6	-2.2
9	10.2	0.4	10.6	-3.9
10	18.0	0.7	18.6	-3.3
11	28.4	1.0	29.6	-4.2
12	42.3	1.5	42.5	-0.5
13	12.2	0.4	12.4	-1.6
Average				-3.2

583

584 ## 4.2 Validating Δx_{max} for the passive failure state

585 The same 13 examples of Table 2 are used here for validating the Δx_{max} required for the
586 passive failure state. While the automatically derived P_{PE} values using mrearth2d (column c2.1
587 in Table 8) deviate from the P_{PE} values derived from the proposed method (c2.5) by only -0.5%
588 (on average), for wall displacement equal to Δx_{max} (c5.3) the mrearth2d P_{PE} values (c9.5) re-
589 vealed also no noticeable difference (average *RD*= -0.3%; column c9.6). The proposed method
590 was used as reference point for calculating all *RD* values in Table 9. In addition to the above,
591 the RS2 results in Table 6 (columns c6.10 to c6.13) also support the validity of the Δx_{max}

592 expression (Equation 4) for the passive state, although, according to the same table, a greater
593 wall displacement seems to offer slightly better prediction; for example a wall displacement
594 equal to $2\Delta x_{max}$ reduces the relative difference to just a few decimal units (avoiding an unnec-
595 essary repetition, the author's prompts to Section 3.2.1). However, as shown later in this sec-
596 tion, the Δx_{max} displacement given be Equation 4 is the correct answer to the problem.

597

598 **Table 9.** Validating Δx_{max} for the passive failure state (case of purely frictional soils).
599

S/N	Proposed method		mrearth2d (automatic)		mrearth2d (for Δx_{max})	
	$P_{PE,I}$ (kN)	Δx_{max} (mm)	P_{PE} (kN)	RD_I (%)	P_{PE} (kN)	RD_I (%)
	c2.5	c6.3	c2.1	c9.4	c9.5	c9.6
1	275.0	28.6	286.0	-4.0	267.1	2.9
2	239.1	23.6	237.7	0.6	233.3	2.4
3	180.7	14.9	171.2	5.3	178.5	1.2
4	146.1	11.7	173.6	-18.8	174.0	-19.1
5	192.6	17.6	201.8	-4.8	205.7	-6.8
6	285.6	29.5	260.2	8.9	266	6.9
7	80.2	6.6	76.3	4.9	77.1	3.9
8	19.6	1.7	20.2	-3.1	19.9	-1.5
9	44.1	3.7	44.2	-0.2	44.3	-0.5
10	78.4	6.6	79.3	-1.1	78.6	-0.3
11	122.6	10.4	123.2	-0.5	121.7	0.7
12	176.5	14.9	174.6	1.1	175.4	0.6
13	39.9	3.0	37.8	5.3	37.9	5.0
Average				-0.5		-0.3

600
601 The validity of Equation 4 was also checked for the case of cohesive-frictional soils. This
602 was done for the same ten passive state examples initially presented in Table 3. The calculated

603 Δx_{max} values are given in column c7.8 of Table 10, while the mrearth2d P_{PE} values corre-
604 sponding to these Δx_{max} values are shown in column c10.7; the P_{PE} values derived automati-
605 cally by the mrearth2d program (column c.3.3) are used as reference values. In this respect, the
606 proposed method gave an average *RD* value equal to 3.2%, while the new runs with mrearth2d
607 and RS2 (for Δx_{max}) as small as -6.6% and 6.2% respectively (columns c10.8 and c10.10).

608 **Table 10.** Validating Δx_{max} for the passive failure state (case of cohesive-frictional soils).

S/N	DATA		mrearth2d (automatic)	Proposed method			mrearth2d (Δx_{max})		RS2 for Δx_{max} (c_m, φ_m, k_h=0)	
	c'	k_h	$P_{PE,I}$	P_{PE}	Δx_{max}	RD_I	P_{PE}	RD_I	P_{PE}	RD_I
	(kPa)	-	(kN)	(kN)	(mm)	(%)	(kN)	(%)	(kN)	(%)
	c3.1	c3.2	c3.3	c3.4	c7.8	c3.5	c10.7	c10.8	c7.11	c10.10
3.0	0	0.2	172.5	180.7	14.9	-4.8	178.4	-3.4	175.9	-2.0
3.1	10		262.7	263.7	25.9	-0.4	268.0	-2.0	252.9	3.7
3.2	20		348.8	340.2	36.9	2.5	385.2	-10.4	331.9	4.8
3.3	30		439.4	425.6	47.9	3.1	490.1	-11.5	411	6.5
3.4	40		536.2	513.0	58.9	4.3	594.7	-10.9	497.5	7.2
3.5	0	0.3	150.7	159.7	12.1	-6.0	152.6	-1.3	155.8	-3.4
3.6	10		241	227.1	21.5	5.8	252.7	-4.9	221.3	8.2
3.7	20		336.5	302.5	31.4	10.1	341.1	-1.4	293.5	12.8
3.8	30		421	382.7	41.7	9.1	435.3	-3.4	370	12.1
3.9	40		509.8	466.2	52.1	8.6	596.0	-16.9	450.4	11.7
Average						3.2		-6.6		6.2

609
610 The interesting observation made in Section 3.2.1 that the RS2 P_{PE} values in Table 6 are
611 very close (i.e. columns c2.2, c6.10 and c6.12 for $\{\varphi',\ k_h, 2\Delta x_{max}\}$, $\{\varphi_m,\ k_h = 0,\ \Delta x_{max}\}$
612 and $\{\varphi_m, k_h = 0,\ 2\Delta x_{max}\}$ respectively), gave rise to further investigating this point. In this
613 respect, three charts have been drawn in Figure 8, all referring to example No 3 (data shown in
614 Table 1). In this respect, Figure 8a presents RS2 results derived conventionally, that is, for
615 $\{\varphi',\ k_h\}$; these results refer to Δx values ranging from 0 to $2\Delta x_{max}$ (with $0.2\Delta x_{max}$ interval,

where Δx_{max} is the analytically calculated maximum wall displacement at $H/2$). Regarding Figure 8b, the only difference is that the RS2 model was solved for $\{\varphi_m, k_h = 0\}$ instead of the $\{\varphi',\ k_h\}$ pair of values. In both cases, Jaky's initial stresses were used (that is, $K_O = 0.5774$). In Figure 8c, the RS2 model of the second case was solved considering the initial stresses for seismic situation derived from the proposed method (K_{OE}= 0.631; recall Equation 1) instead of Jaky's ones. The passive earth pressure distribution for seismic situation derived from the proposed method and the initial stresses have also been drawn on these three charts, playing the role of theoretical boundaries.

As it can be inferred from Figure 8a, the $a = 0$ RS2 curve (representing the at-rest state) is erroneously below Jaky's initial stresses (it is reminded that Jaky's coefficient was used as input data in RS2), raising subsequently queries for the validity of the other curves of the same chart; besides, this curve rather prompts to the active state. A passive pseudostatic model, however, may need a wider model for avoiding the phenomenon of stresses bouncing on the back geometry boundary in the finite element model and returning to the wall (action and reaction problem). Extending the width of the RS2 model from $X = 6H$ to $X = 9H$ (recall the geometry in Figure 4a), nothing essentially changed.

In Figure 8b (case of φ_m and $k_h = 0$), on the other hand, Jaky's theoretical earth pressure at-rest distribution coincides perfectly with the respective distribution derived from RS2 (use of Jaky's coefficient as input value). In this case the seismic information is already included in the φ_m value of the seemingly static model. As shown in Figure 8b, failure occurs when the wall movement reaches the predicted Δx_{max} value. However, although the numerical earth pressure distribution corresponding to passive failure has effectively been found, while moreover the earth pressures at-rest have successfully been predicted by RS2, it is noted that, only

639 the earth pressures at failure in Figure 8b are actually correct. In the figure in question there is
640 no compatibility between the static pressures for $\Delta x = 0$ and the dynamic pressures for Δx_{max};
641 consequently, any intermediate state is "more static - less dynamic" if α is closer to zero and
642 "more dynamic - less static" when α approaches 1. This common error in engineering practice,
643 however, can be avoided using the earth pressure coefficient for seismic situation of Equation
644 1, with the intermediate earth pressure curves to lie within the two logical boundaries, the at-
645 rest state boundary for seismic situation and the passive state for seismic situation boundary
646 (Figure 8c).

647 From the above it is inferred that despite the fact that the numerical P_{PE} value is effectively
648 calculated in every case, the $\{c_m, \varphi_m, k_h = 0\}$ approach in finite element analysis presents the
649 indisputable advantage over the conventional $\{c', \varphi',\ k_h\}$ approach of effectively calculating
650 the intermediate earth pressures.

651 A α versus P_{PE} chart is given in Figure 9, extracted from the curves of Figure 8. Each point
652 on the RS2 curves in Figure 9 corresponds to the chart area bounded by the respective RS2
653 earth pressure distribution in Figure 8 and the z-axis. As shown, in the $\{\varphi_m, k_h = 0, K_{OE}\}$ case,
654 the RS2 curve starts from the P_{OE} value derived from the proposed method (compare the 56.8
655 kN analytical value with the 57.4 kN numerical one) and tends towards the P_{PE} value derived
656 again from the proposed method as Δx increases (please compare the 180.4 kN value with the
657 177.3 kN one respectively; 175.6 kN at Δx_{max}). The fourth (lower) curve in Figure 9 refers
658 also to the conventional way of modelling with finite elements, but, in this respect, a wider
659 RS2 model was used ($X = 9H$ instead of $X = 6H$; recall Figure 4a); all other parameters care-
660 fully remained the same, including mesh density. As shown, extending the horizontal geometry
661 by 50%, the new model resulted to minor changes in the intermediate earth pressures.

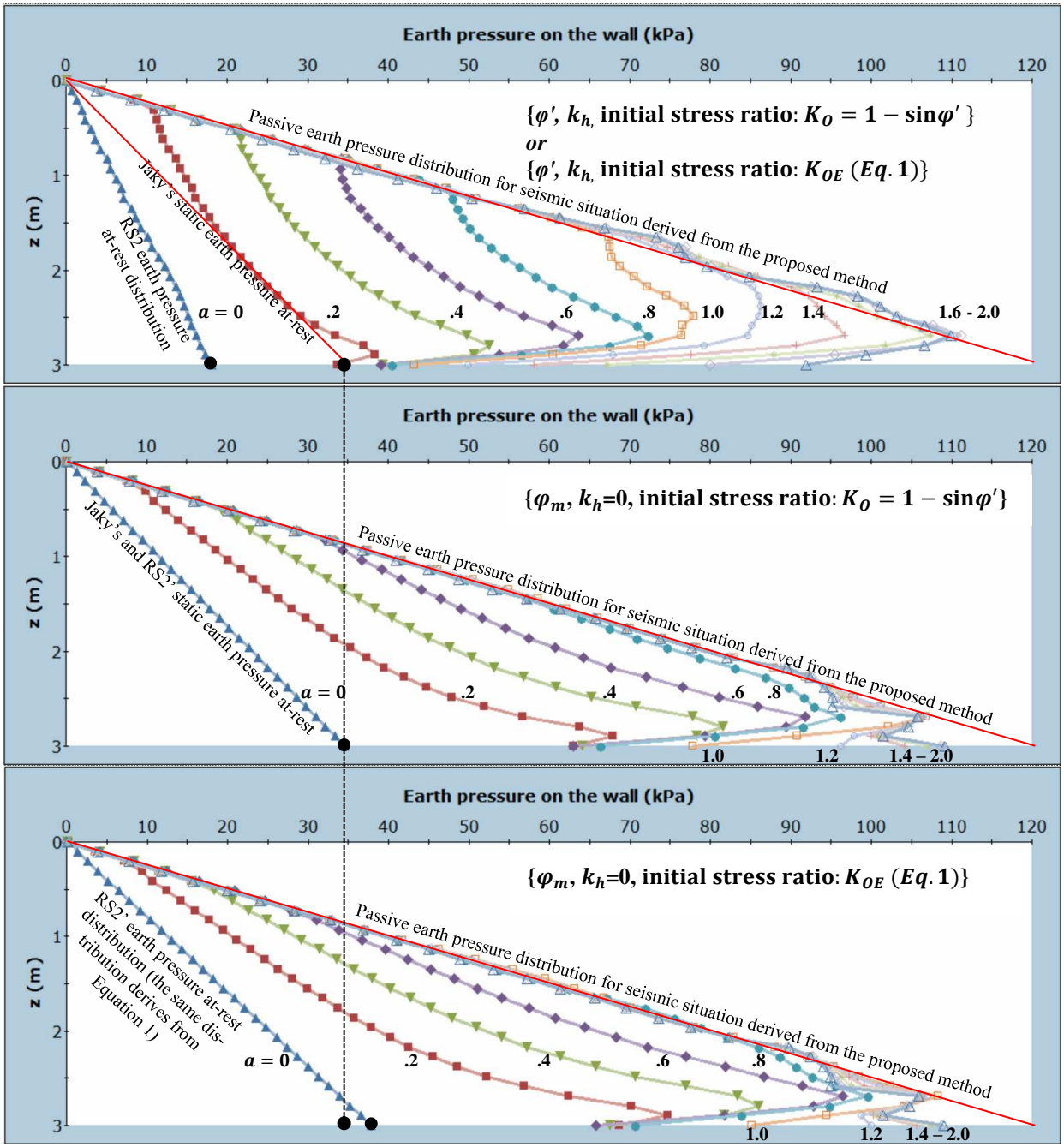

Figure 8. Example No3 solved with RS2 for various displacement steps ($\Delta x = a \cdot \Delta x_{max}$, $a = 0, 0.2, \ldots, 2$). *Model solved for (a)* φ', k_h and Jaky's initial stresses (similar results are obtained using the initial stresses derived from the proposed method), (b) φ_m, k_h=0 and Jaky's initial stresses, and (c) φ_m, k_h=0 and the initial stresses derived from the proposed method.

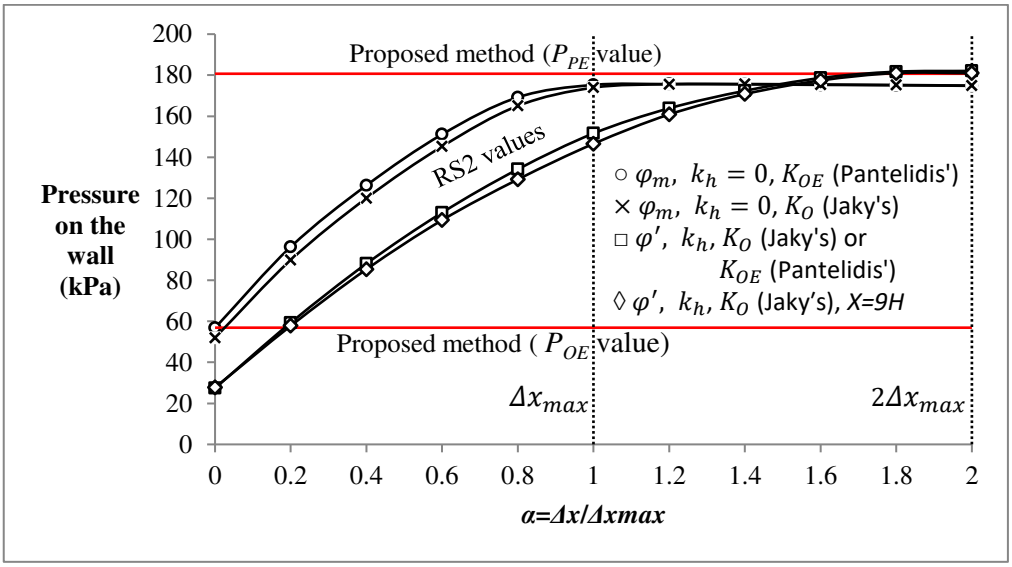

669

670 **Figure 9.** Pressure on the wall versus $a = \Delta x/\Delta x_{max}$ curves for various cases (chart refer-
671 ring to Example 3 and the earth pressure on the wall versus z curves of Figure 8).

672

673 According also to Figure 9, it seems that the use of the proposed K_{OE} coefficient in RS2 has
674 not seriously affected the intermediate earth pressures. However, this is because the static $K_O =$
675 0.5774 value happens to be very close to the dynamic K_{OE}= 0.631 value. Greater k_h values
676 and/or soils' cohesion (if present) may greatly affect the earth pressure at-rest coefficient and
677 thus, the intermediate earth pressures.

678 Finally, the following simple relationship between $\Delta x_{max,P}$ and $\Delta x_{max,A}$ (i.e. Δx_{max} for mo-
679 bilizing the passive and active failure state respectively) derives from Equation 4:

680 $$\lambda_\Delta = \frac{\Delta x_{max,P}}{\Delta x_{max,A}} = \frac{K_{PE} - K_{OE}}{K_{OE} - K_{AE}} \quad (20)$$

681 For a wall retaining cohesionless soil with $\varphi' = 30^o$ and obeying the main Rankine's [13]
682 assumptions, $\lambda_\Delta = 15$. The λ_Δ ratio decreases as k_h increases (e.g., λ_Δ =9.97 and 5.26 for
683 $k_h = 0.3$ and 0.5 respectively; $k_v = 0$).

5 Conclusions

This paper presents an exhaustive comparison of the earth pressure methods included in EN1998-5:2004, prEN1998-5:2022 draft standard and AASHTO standards, against contemporary centrifuge tests, finite elements, and the method proposed by the first author in 2019. Both EN1998-5:2004 and AASHTO standards have adopted the Mononobe-Okabe method, the first replacing the negative root with unity when $\varphi' - \theta_1 - a_s < 0$ (it stands for the active state, only; no provision exists for the negative root in the passive state when $\varphi' - \theta_1 + a_s < 0$), while the second using the half peak ground acceleration, thus, recognizing its conservatism. It is noted that, the method replacing the Mononobe-Okabe one in prEN1998-5:2022 draft standard also presents the same negative root problem for $\varphi' - \theta_1 \mp a_s < 0$ (the minus sign is for the active state while the plus sign for the passive state). It is mentioned that under Rankine's assumptions, the proposed continuum mechanics approach returns Rankine's active earth pressure stresses for c-phi soils, while under Jaky's assumptions, it returns the well-known $K_o = 1 - \sin\varphi$' expression; both cases derive from the generalized equation of Equation 15, just changing the arithmetic value of the controlling parameter m.

The calibration of a well-known method by an association such as AASHTO is an important fact, and a point that attracted the interest of the authors. In this respect, it is remarkable how this empirical correction by AASHTO sends the Mononobe-Okabe curves for the active state over the fully analytical ones derived from the proposed method. However, this correction does not work for the full range of phi values as well as for the passive state.

For the numerical comparison carried out in the present study as well as the numerical validation of the Δx_{max} displacement of wall, and the mobilized shear strength values (c_m, φ_m) of soil, in total 157 numerical cases with two finite element programs (Rocscience's RS2 and

mrearth2d) were run. All results, clearly show that the EN19985-5:2004 method gives conservative to excessively conservative active earth pressure values, AASHTO's empirical calibration fairly good behavior, while prEN1998-5:2022 excessively conservative values. For the passive state, all methods included in the above-mentioned standards, return unreliable and also unconservative results. On the other hand, the results obtained by the proposed method show a remarkable agreement with the respective ones obtained by the finite element method. In addition to this, as shown, it is possible a pseudo-static earth retention analysis to be replaced by an equivalent static analysis, just substituting the shear strength values (c', φ') of soil of the original problem with the mid-height mobilized ones (c_m, φ_m), obtaining more stable finite element results; besides, the $\{c_m, \varphi_m\}$ values contain the seismic information. Indeed, the very same procedure works also for toe failures in c-phi slope stability problems; the application of the mobilized shear strength values to slopes, is still under investigation. In essence, the mobilized values are nothing else than the shear strength values for the seismic situation, and the mid-height values are representative values.

The under-review earth pressure coefficients have also been compared against contemporary centrifuge test results of two independent studies and an in-situ measurement with press-in cell (third study). In this respect, the agreement of the results of the proposed method could be described as perfect. The comparison also revealed very limited effectiveness for the various methods included in the under-examination design standards.

It is finally mentioned that all experimental, numerical, and analytical results lead to the same conclusion that the Mononobe-Okabe method (EN19985-5:2004) gives conservative active earth pressure values, and excessively conservative values for *PGA* values greater than 0.4g. This is a significant finding, as in the draft standard prEN1998-5:2022 the Mononobe-

730 Okabe method has been replaced by an even more conservative method which, indeed, contains
731 the same "negative root" problem as Mononobe-Okabe. For the passive state, the two Eurocode
732 8-5 methods not only return unreliable results but also unconservative.

733 **Notation**

734 $a = \Delta x/\Delta x_{max}$

735 a_s= the inclination of the ground surface

736 β = the back face inclination angle of the structure with respect to vertical

737 γ= the unit weight of soil

738 ΔP_{AE}=the seismic increment of active earth pressure

739 $\Delta K = K_{OE} - K_{AE}$ or $K_{PE} - K_{OE}$

740 Δx = the wall displacement

741 Δx_{max}= the lateral displacement of wall corresponding to the active or passive state; the sym-
742 bols $\Delta x_{max,A}$ and $\Delta x_{max,P}$ are also used for the active and passive state respectively

743 δ= the friction angle between the wall and the soil

744 $\theta_1 = \arctan(k_h/(1 - k_v))$

745 $\theta_2 = arctan(k_h)$

746 $\xi = (1 - 3m)/\big(m \cdot (1 + m)\big)$

747 σ_{AE}, σ_{PE} or σ_{OE} = the active, passive or at-rest earth pressure in the seismic situation

748 φ'= the effective internal friction angle of soil

749 φ_m= the mobilized friction angle of soil (for its calculation see [1])

750 ψ= the apparent inclination of the gravity field in the seismic situation

751 c'= the effective cohesion of soil

752 c_m= the mobilized cohesion of soil (for its calculation see [1])

753 H= the height of the retaining soil

754 K_A =Rankine's coefficient of active earth pressure

755 Ko = Jaky's (static) coefficient of earth pressure at-rest

756 K_{AE}, K_{PE} or K_{OE} = the active, passive or at-rest coefficients of earth pressure in the seismic
757 situation

758 K_{Liq}= coefficient of earth pressure during liquefaction of soil ($K_{Liq} = 1$)

759 k_h= the seismic coefficient of horizontal acceleration

760 k_v= the seismic coefficient of vertical acceleration (if negative, the vertical pseudo-static force
761 acts downwards, i.e. it increases the unit weight of soil, $(1 + k_v)\gamma$)

762 M-O= Mononobe-Okabe method

763 m=real positive number ranging from 1 to $+\infty$

764 P_{AE}, P_{PE} or P_{OE} = the active, passive or at-rest resultant earth pressure force in the seismic
765 situation

766 *PGA*= peak ground acceleration

767 *SMF*=Strength Mobilization Factor

768 z= the depth where the earth pressure is calculated

769 **Data availability statement**

770 All data generated or used during the study are available from the corresponding author by
771 request.

CRediT authorship contribution statement

Lysandros Pantelidis: Conceptualization; Methodology; Software; Formal analysis; Investigation; Resources; Writing - original draft; Writing - review & editing; Visualization; Supervision, **Panagiotis Christodoulou:** Software (mrearth2d); Visualization.

Declaration of Competing Interest

The authors declare that they have no known competing financial interests or personal relationships that could have appeared to influence the work reported in this paper.

References

1. Pantelidis L (2019) The Generalized Coefficients of Earth Pressure: A Unified Approach. Appl Sci 9:5291
2. Jaky J (1948) Pressure in silos. In: Proceedings of the 2nd International Conference on Soil Mechanics and Foundation Engineering ICSMFE. London, pp 103–107
3. Pantelidis L (2022) Shaft resistance capacity of axially loaded piles in cohesive-frictional soils under static or pseudo-static conditions based on ground parameters. ResearchSquare (preprint): https://doi.org/10.21203/rs.3.rs-1986330/v1
4. Pantelidis L (2022) Designing embedded retaining walls relying on the Generalized Coefficient of Earth Pressure and the elastic beam theory. ResearchSquare (preprint): https://doi.org/10.21203/rs.3.rs-2132476/v2
5. Mononobe N, Matsuo H (1929) On the determination of earth pressures during earthquakes. In: World Engineering Congress. Tokyo
6. Okabe S (1926) General theory of earth pressure. Japan Soc Civ Eng 12:
7. Kapila J (1962) Earthquake resistant design of retaining walls. Proc 2nd Earthq Symp

794 97–108
795 8. EN1998-5:2004 (2004) Eurocode 8 - Design of structures for earthquake resistance -
796 Part 5: Geotechnical aspects, foundations, retaining walls and underground structures
797 9. AASHTO (American Association of State Highway and Transportation Officials)
798 (2010) LRFD Bridge Design Specifications, 5th ed. Washington, DC
799 10. prEN1998-5:2022 (2022) Eurocode 8 - Earthquake resistance design of structures - Part
800 5: Geotechnical aspects, foundations, retaining walls and underground structures (draft
801 standard)
802 11. Lew M, Sitar N, Al Atik L, et al (2010) Seismic earth pressures on deep building
803 basements. In: Structural Engineers Association of California, Proceedings of the
804 Annual Convention
805 12. USACE US (1989) Army Corps of Engineers. Engineering and design of retaining and
806 flood walls. EM 1110-2-2502
807 13. Rankine WJM (1857) II. On the stability of loose earth. Philos Trans R Soc London 9–
808 27
809 14. Coulomb CA (1776) An attempt to apply the rules of maxima and minima to several
810 problems of stability related to architecture. Mémoires l'Académie R des Sci 7:343–382
811 15. Bell AL (1915) The lateral pressure and resistance of clay and the supporting power of
812 clay foundations. In: Minutes of the Proceedings of the Institution of Civil Engineers.
813 Thomas Telford-ICE Virtual Library, pp 233–272
814 16. Agusti GC, Sitar N (2013) Seismic Earth Pressures on Retaining Structures in
815 Cohesionless Soils
816 17. Sitar N, Mikola RG, Candia G (2012) Seismically induced lateral earth pressures on

retaining structures and basement walls. In: Geotechnical Engineering State of the Art and Practice: Keynote Lectures from GeoCongress 2012. pp 335–358

18. Mikola RG, Candia G, Sitar N (2016) Seismic earth pressures on retaining structures and basement walls. J Geotech Geoenvironmental Eng 142:4016047

19. Wagner N, Candia G, Mikola RG, Sitar N (2017) Seismic earth pressures – Experiments and Analyses. 3rd Int Conf Perform Based Des

20. Sitar N, Al Atik L (2008) Dynamic centrifuge study of seismically induced lateral earth pressures on retaining structures. In: Geotechnical Earthquake Engineering and Soil Dynamics IV. pp 1–11

21. Mikola RG, Sitar N (2013) Seismic Earth Pressures on Retaining Structures in Cohesionless Soils (Report No. UCB GT 13-01, March 2013). California Department of Transportation, Sacramento CA

22. Finn WD (1963) Boundary Values Problems of Soil Mechanics. J Soil Mech Found Div 89:39–72

23. Fragaszy RJ, Dendy G, Higgins JD (1987) Seismic response of tieback retaining walls, Phase I. Pullman, WA

24. Lew M, Sitar N, Atik L Al (2010) Seismic earth pressures: Fact or fiction? In: Earth Retention Conference 3. pp 656–673

25. Wagner N, Sitar N (2016) Seismic Earth Pressures on Deep Stiff Walls. In: Geotechnical and Structural Engineering Congress 2016. pp 499–508

26. Al Atik L, Sitar N (2010) Seismic Earth Pressures on Cantilever Retaining Structures. J Geotech Geoenvironmental Eng 136:1324–1333. https://doi.org/10.1061/(ASCE)GT.1943-5606.0000351

840 27. Gazetas G, Psarropoulos PN, Anastasopoulos I, Gerolymos N (2004) Seismic behaviour
841 of flexible retaining systems subjected to short-duration moderately strong excitation.
842 Soil Dyn Earthq Eng 24:537–550
843 28. Psarropoulos PN, Klonaris G, Gazetas G (2005) Seismic earth pressures on rigid and
844 flexible retaining walls. Soil Dyn Earthq Eng 25:795–809
845 29. Al Atik L, Sitar N (2007) Development of improved procedures for seismic design of
846 buried and partially buried structures. Pacific Earthquake Engineering Research Center
847 30. Fenton GA., Griffiths D V. (2008) Risk assessment in geotechnical engineering. Wiley,
848 Hoboken, NJ, USA
849 31. Griffiths D V, Fenton GA, Ziemann HR (2008) Reliability of passive earth pressure.
850 Georisk 2:113–121
851 32. Christodoulou P, Pantelidis L, Gravanis E (2019) The Effect of Targeted Field
852 Investigation on the Reliability of Earth-Retaining Structures in Active State. Appl Sci
853 9:4953. https://doi.org/10.3390/app9224953
854 33. Christodoulou P, Pantelidis L, Gravanis E (2020) The Effect of Targeted Field
855 Investigation on the Reliability of Earth-Retaining Structures in Passive State: A
856 Random Field Approach. Geosciences 10:110.
857 https://doi.org/10.3390/geosciences10030110
858 34. Smith I, Griffiths D (2004) Programming the finite element method, 4th ed. John Wiley
859 & Sons, Chichester, West Sussex
860 35. Lindgård, A., Strømme Ofstad C (2016) An evaluation of methods to determine Ko clays
861 - Literature study and pilot experiments conducted at Tiller in connection with NGTS,
862 Project Thesis: TBA4510. Trondheim,

863 36. Mayne PW, Kulhawy FH (1982) K0-OCR relationships in soil. J Geotech Eng 108
864 (GT6):851–872
865 37. Seed HB, Whitman RV (1970) Design of earth retaining structures for dynamic loads.
866 In: ASCE Specialty Conf.-Lateral Stresses in the Ground and Design of Earth Retaining
867 Structures. pp 103–147
868 38. Olson SM, Hashash YMA, Muszynski MR, Phillips C (2017) Passive wedge formation
869 and limiting lateral pressures on large foundations during lateral spreading. J Geotech
870 Geoenvironmental Eng 143:4017027
871 39. Gu X, Wu D, Zuo K, Tessari A (2022) Centrifuge Shake Table Tests on the Liquefaction
872 Resistance of Sand with Clayey Fines. J Geotech Geoenvironmental Eng 148:.
873 https://doi.org/10.1061/(ASCE)GT.1943-5606.0002708
874 40. Lee C-J, Chen H-T, Lien H-C, et al (2014) Centrifuge modeling of the seismic responses
875 of sand deposits with an intra-silt layer. Soil Dyn Earthq Eng 65:72–88.
876 https://doi.org/10.1016/j.soildyn.2014.06.002
877